Title

Neuroprotective role of Hippo signaling by microtubule stability control in *C. elegans*

Short title: Hpo pathway maintains neuronal integrity

Authors

Hanee Lee[1], Junsu Kang[1†], Sang-Hee Lee[1‡], Dowoon Lee[1], Christine H. Chung[1], Junho Lee[1*]

Affiliations

[1] Department of Biological Sciences, Institute of Molecular Biology and Genetics,

Seoul National University, Seoul, 08826, South Korea

* Correspondences to

Junho Lee

Department of Biological Sciences, Seoul National University

Gwanak-ro 1, Gwanak-gu, Seoul, 08826, South Korea

elegans@snu.ac.kr

[†] Present address: Department of Cell and Regenerative Biology, University of Wisconsin School of Medicine and Public Health, University of Wisconsin–Madison, Madison, WI 53705, USA

‡ Present address: Korea Basic Science Institute, Ochang, Cheongju, Chungbuk, 28119, South Korea

Abstract

The evolutionarily conserved Hippo (Hpo) pathway has been shown to impact early development and tumorigenesis by governing cell proliferation and apoptosis. However, its post-developmental roles are relatively unexplored. Here, we demonstrate its roles in post-mitotic cells by showing that defective Hpo signaling accelerates age-associated structural and functional decline of neurons in *C. elegans*. Loss of *wts-1*/LATS resulted in premature deformation of touch neurons and impaired touch responses in a *yap-1/*YAP-dependent manner. Decreased movement as well as microtubule destabilization by treatment with colchicine or disruption of microtubule stabilizing genes alleviated the neuronal deformation of *wts-1* mutants. Colchicine exerted neuroprotective effects even during normal aging. In addition, the deficiency of a microtubule-severing enzyme *spas-1* also led to precocious structural deformation. These results consistently suggest that hyper-stabilized microtubules in both *wts-1*-deficient neurons and normally aged neurons are detrimental to the maintenance of neuronal structural integrity. In summary, Hpo pathway governs the structural and functional maintenance of differentiated neurons by modulating microtubule stability, raising the possibility that the microtubule stability of fully developed neurons could be a promising target to delay neuronal aging. Our study provides potential therapeutic approaches to combat age- or disease-related neurodegeneration.

Keywords

Neuronal aging/Neuronal integrity/Hippo pathway/microtubule/*C. elegans.*

Introduction

Neurons perceive extracellular signals and transmit the information to other cells, often over long distances. For this to happen, neuronal cells extend their axons and dendrites from 1 μm to more than 1 m and must maintain an intact morphology throughout their lifetime. The long, elaborate neuronal structures are vulnerable to degeneration associated with organismal aging or pathological conditions. Structural abnormalities and the consequent functional decline are hallmarks of aged neurons or pathological neurons affected by neurodegenerative diseases (Yankner et al. 2008; Bishop et al. 2010; Fjell and Walhovd 2010). Several studies have shown that the aged brain exhibits structural abnormalities such as synaptic loss, neuronal sprouting and restructuring, rather than neuronal cell death (reviewed in (Yankner et al. 2008)).

Microtubules form essential cytoskeletal structures for most eukaryotic cells. In neurons, they serve as structural struts that allow the neuron to develop and maintain a specific shape (Barnes and Polleux 2009; Marin et al. 2010). They also act as railroads for motor proteins that deliver cellular cargo from cell bodies to distal axons (Hirokawa et al. 2010; Maday et al. 2014), as well as seeds for microtubule polymerization (Job et al. 2003). Microtubules of varying lengths are observed in neurons, and they can be both stable and dynamic. Numerous studies have suggested that both hyper- or un-stable microtubules are harmful for maintaining neuronal morphology as the imbalance in microtubule dynamics contributes to neurological diseases (reviewed in (Dubey et al. 2015)). Thus, microtubule regulators have been implicated in a number of human diseases (Dubey et al. 2015; Matamoros and Baas 2016) and signaling pathways including Notch pathway have been proposed as pharmaceutical targets for cytoskeletal protection of postnatal neurons (Bonini et al. 2013). Microtubule dynamics in normal neuronal aging, on the other hand, are poorly understood at the organismal level.

The neurons of *Caenorhabditis elegans* provide a valuable model system because they share

fundamental characteristics with mammalian neurons in terms of their molecular basis and functions. Major genetic pathways governing early neuronal development such as neuronal cell migration or polarization were initially identified from numerous studies on *C. elegans* (Hedgecock et al. 1990; Wadsworth et al. 1996; Culotti and Merz 1998; Ikegami et al. 2004). Additionally, *C. elegans* neurons could be utilized to understand the molecular mechanism of neuronal aging as they demonstrate age-associated structural and functional deterioration. In particular, touch receptor neurons (TRNs), comprising 2 ALM, AVM, 2 PLM, and PVM, show the most prominent decline in structure and function with aging (Pan et al. 2011; Tank et al. 2011; Toth et al. 2012). In aged animals, TRNs have highly wavy or ectopically branched processes, misshaped cell bodies with abnormal morphology or outgrown processes. Moreover, *C. elegans* exhibits gradual decreases in touch responses as they age (Tank et al. 2011). DAF-2/IGF pathway, JNK/MAPK pathway and membrane activity of TRNs have been identified to influence the speed of touch neuronal aging by modulating whole organismal senescence or cell-autonomous functions (Pan et al. 2011; Tank et al. 2011; Toth et al. 2012).

The Hippo (Hpo) kinase signaling pathway, which is evolutionarily conserved across animal species, plays a pivotal role in the regulation of tissue size homeostasis (Harvey et al. 2013). It regulates cell proliferation and apoptosis during early development and tumorigenesis. When the Hpo pathway is active, LATS, the core kinase of the pathway, phosphorylates and inhibits the nuclear localization of YAP, a transcriptional co-activator. In the nucleus, YAP regulates target gene expression through interaction with the TEAD transcription factor (Zhao et al. 2007; Zhao et al. 2008). The dysregulation of this pathway promotes uncontrolled cell proliferation, leading to tumorigenesis and developmental problems (Huang et al. 2005; Zhao et al. 2007; Harvey et al. 2013; Zheng and Pan 2019). In *C. elegans*, core components and their genetic interaction of the Hpo pathway are conserved. Inhibition of YAP-1/YAP by upstream WTS-

1/LATS is needed for the maintenance of apicobasal membrane polarity of the developing intestine (Kang et al. 2009; Lee et al. 2019). The functions of the Hpo pathway in growth control are extensively established; however, its post-developmental functions are relatively unknown.

Here, we establish a novel genetic animal model that reveals the postnatal roles of the Hpo pathway in the differentiated neurons. Loss of *wts-1* leads to premature decline of TRNs both in structure and function and downstream effectors, *yap-1* and *egl-44,* are required in this phenomena. We employ genetic and chemical approaches to elucidate the cellular and molecular mechanisms by which *wts-1*-deficient TRNs lead to a premature deformation. Our results demonstrate that hyper-stabilized microtubules of the *wts-1* mutant or aged organism are responsible for neuronal deformation. The fact that loss of *spas-1*, a putative microtubule-severing enzyme, accelerates onset of age-associated neuronal deformation also supports the contribution of hyper-stabilized microtubules in neuronal failures. Our study unveils the post-developmental functions of the Hpo pathway in the maintenance of neuronal integrity and highlights the importance of neuronal microtubule status in cellular aging and clinical approaches.

Results

wts-1 mutant showed impaired structure of touch receptor neurons

A previous study demonstrated that the intestinal Hpo pathway is essential for the proper development of the intestinal lumen and loss of *wts-1*, the core kinase of the pathway, leads to early larval death (Lee et al. 2019). To define the non-intestinal roles of the Hpo pathway in *C. elegans*, we used the mosaic *wts-1* mutant system of which larval lethality was overcame with

the intestine-specific expression of WTS-1. Since *wts-1* activity in all tissues except the intestine is absent in this system, hereafter we will refer to it as the *wts-1* mutant shortly.

We observed that the *wts-1* mutants showed extremely distinctive abnormalities in the morphology of touch receptor neurons (TRNs). In the wild-type, ALM and its posterior homolog PLM extended their neuronal processes along the anterior-posterior axis and maintained structural integrity during adolescence (Fig. 1A, B). However, the *wts-1* mutant-ALM and PLM exhibited ectopic swelling/waviness and branching (Fig. 1A, B), and other various deformations, including extended or shortened distal processes or outgrowth of processes from the cell body (somatic outgrowth) (Supplemental Fig. S1A, B). Atypical structures of other TRNs, AVM and PVM, were also found in the mutants (Supplemental Fig. S1C, D), indicating that *wts-1* is essential in mechanosensory neurons. As ALM and PLM defects were much more severe, frequent and easier to observe, we focused on these neurons for further study.

TRNs of *C. elegans* develop rapidly in their early life and govern escape behaviors in response to aversive stimuli (Chalfie et al. 1985). ALM and PLM complete their development during embryogenesis, whereas AVM and PVM develop until the first larval stage (L1) (Chalfie et al. 1985). To determine whether *wts-1* is required for the development or maintenance of TRNs, neuronal morphology of early larva was analyzed. The *wts-1* mutant had intact, unaltered neuronal processes of ALM and PLM at the very early L1 stage and the frequency of abnormal neurons gradually increased as the worms grew (Fig. 1C, D). At the fourth larval (L4) stage, 98.89% of ALM and 84.44% of PLM, respectively, showed at least one morphological abnormality in the mutant whereas they maintain intact structures in the wild-type (Fig. 1D). Among the abnormalities, ectopic swelling and branching on the processes were the most common (Supplemental Fig. S1E, F), followed by extension of the distal process and somatic

outgrowth of the cell body (Supplemental Fig. S1G, H). All these structural deformations were gradually increased. Ectopic swelling or branching occurred multiple places in a single process and the number of swelling/branching also increased as the worms grew (Supplemental Fig. S1I).

To determine whether *wts-1* acts in the structural maintenance of neurons generally or TRNs specifically, we analyzed the morphologies of other neurons in the mutants. Dopaminergic, GABAergic, and cholinergic neurons were found to maintain structures comparable with those of the wild-type at the same age (Supplemental Fig. S1J, K). It is noteworthy that ALN, a cholinergic neuron that extends its process in association with ALM (White et al. 1986), preserved their structural integrity in the mutants (Supplemental Fig. S1J). Thus, we concluded that the loss of *wts-1* leads to wide range of structural deformities specifically in TRNs and that this deformity is a matter of maintenance, rather than development of the structures.

wts-1 deficiency causes TRNs to deteriorate its structure and function

TRNs govern the aversive movements of worms in response to gentle body touches (Chalfie et al. 1985). To determine whether structurally deformed TRNs of *wts-1* affect neuronal functions, we measured gentle touch responses of the mutant. At the L4 stage, control worms responded to almost every gentle touch (9.40 responses/10 touches), whereas *wts-1* mutants responded to 60% of stimuli (6.31/10) (Fig. 1E). On the first day of adulthood (1DA), control worms showed slightly decreased touch responses compared with the L4 stage (8.25/10), whereas *wts-1* mutants displayed more impaired responses (5.57/10) (Fig. 1E).

The structural and functional decline in the *wts-1* mutants is very similar with phenotypes of normally aged animals. Morphological alteration and consequent functional decline are

typically observed in the aged nervous system across the animal kingdom (Yankner et al. 2008; Bishop et al. 2010; Fjell and Walhovd 2010). Aging of human brain in the absence of disease is often accompanied by structural deformation, such as dendritic restructuring, neuronal sprouting and synaptic losses, rather than severe neuronal degeneration or cell death (Yankner et al. 2008). Consistently, the *C. elegans* nervous system exhibits age-associated structural deformation. Among several neurons, TRNs exhibited the most robust decline in the structure and function during aging (Pan et al. 2011; Tank et al. 2011; Toth et al. 2012). Structural abnormalities of ALM or PLM appear from the 4th day of adulthood and occur in almost every individual after the 15th day of adulthood (Toth et al. 2012). According to our observations, the degree of morphological deformation of the L4 stage *wts-1* was similar to that of the aged wild-type worms on the 15th day of adulthood. These results suggest that loss of *wts-1* leads to structural and functional impairment of TRNs precociously.

yap-1 and *egl-44* suppress premature deformation of *wts-1* TRNs

To determine whether *yap-1* acts downstream of *wts-1* in this phenomenon, we assessed genetic interaction of *yap-1* and *wts-1* mutant. In contrast to the *wts-1* mosaic mutant, the *wts-1; yap-1* mutant could survive without intestinal WTS-1 expression as previously reported (Lee et al. 2019) and displayed intact neuronal processes without any swelling or branching (Fig. 2A). Introduction of a mutation in *egl-44*, which is the worm homolog of TEAD and functions downstream of *wts-1* along with *yap-1* in the developing intestine (Lee et al. 2019), was also sufficient to suppress the structural abnormalities of *wts-1* TRNs (Fig. 2A). To better understand the basic features of structural dis-integrity in the *wts-1* mutant and mitigating effects of the *yap-1* mutation, we examined TRNs from each genetic background using electron microscopy. In wild-type TRNs, multiple microtubules with characteristic spherical shapes

were observed (Fig. 2C). The number of microtubules present in cross sections of control ALM was comparable to the previous report (Chalfie and Thomson 1979) (n = 39, 48, 55, respectively (Supplemental Fig. S2B)). In contrast, in the *wts-1* mutant ALM, the number of microtubules significantly decreased (n = 16, 4, 18, respectively (Supplemental Fig. S2C)) and the morphology was also irregular and non-spherical (Fig. 2C). Consistent with our finding using a fluorescence marker, the abnormalities in the number and shape of microtubules of TRNs were restored in the *wts-1; yap-1* mutant (n = 24, 30, 44, respectively (Supplemental Fig. S2D)) (Fig. 2C). The loss of *yap-1* also restored the impaired touch responses of the *wts-1* mutant. In comparison with the *wts-1* mutant, touch responses of the *wts-1; yap-1* double mutant were significantly rescued (Fig. 2D, E).

Furthermore, to rule out the possibility that the ameliorating effect of *yap-1* mutation on neuronal aging was an indirect result of the delayed organismal aging, we measured the lifespan of each mutant. The *wts-1* mutant had a shorter lifespan than the wild-type, suggesting that prematurely deformed neurons of the *wts-1* mutant were probably due to accelerated organismal aging (Fig. 2F). However, given that the *wts-1; yap-1* mutant with restored neurons had a slightly shorter lifespan than the *wts-1* mutant (Fig. 2F) and only TRNs were affected in the mutant, premature deformation of the *wts-1* neurons appeared to be a touch neuron-specific event, rather than being associated with whole body.

The Hpo pathway acts in a cell autonomous manner to maintain TRNs integrity

To ascertain whether these function of WTS-1 is cell-autonomous or not, we knock-downed WTS-1 selectively in TRNs by injecting tissue-specific-RNAi constructs into wild-type animals as previously described (Esposito et al. 2007). *S*ense and *a*ntisense constructs

corresponding to a region containing kinase domain (sas1) or many exons (sas2) of the *wts-1* gene were expressed under *mec-4* promoter which is specifically active in all six TRNs (Fig. 3A). For each construct, three transgenic lines were obtained and TRNs structure of these lines were compared to that of the controls only harboring the transgenic marker, P*unc-122*::RFP. While the control did not have any abnormalities of TRNs, every transgenic lines showed significant disintegration of TRNs such as ectopic neuronal swellings or shortened neuronal processes as seen in *wts-1* mutant at L4 stage (Fig. 3B–D). These neuronal abnormalities induced by TRNs-specific *wts-1* RNAi was consistently observed in 1DA and the penetrance of phenotype was slightly increased (Supplemental Fig. S3A–C). These results documented that WTS-1 functions in TRNs to maintain intact neuronal structures.

Regarding the action mechanism of the Hpo pathway in the cells, YAP-1 likely acts in the same cell with WTS-1. To clarify this, we rescued YAP-1 activity specifically in TRNs of *wts-1; yap-1* mutants. Touch neuronal expression of YAP-1 using a *mec-4* promoter was sufficient to re-emerge ectopic neuronal swelling in the *wts-1; yap-1* mutants. Approximately 40% of transgenic worms exhibited ectopic swelling and branching on ALM or PLM. In contrast, siblings containing no transgene preserved intact neuronal processes (Fig. 3E, F).

Overexpression of YAP is commonly observed in many human cancers and is associated with poor prognosis of the diseases (Liu et al. 2013; Yuan et al. 2016; Guo et al. 2019). Inducible overexpression of YAP is sufficient to increase liver size in mice through transcriptional regulation of downstream genes that activate cell proliferation (Dong et al. 2007). To see if TRNs-specific overexpression of YAP-1 is sufficient to induce neuronal abnormalities, we overexpressed P*mec-4*::YAP-1 in a wild-type and found that overexpressing YAP-1 causes multiple neuronal defects in a dose-dependent manner (Fig. 3G–J). Lower expression of YAP-1 (1 ng/μl, final concentration in the injection mixture) rarely affects neuronal structure of ALM

or PLM (Fig. 3I, J). Transgenic worms injected P*mec-4*::YAP-1 at 10 ng/μl final concentration slightly, but not significantly, elevated neuronal defects of TRNs. However, higher expression of YAP-1 in TRNs (50 or 100 ng/μl) resulted neuronal defects similar to TRNs-specific *wts-1* knockdown (Fig. 3G–J). It seems that endogenous WTS-1 could inhibits overexpressed YAP-1 at lower concentration along with endogenous YAP-1, however, fails to inhibit overexpressed YAP-1 at higher levels. These results demonstrated that *wts-1* and *yap-1* act in a cell-autonomous manner to induce structural disintegration of TRNs; thus, proper regulation of YAP-1 activity by WTS-1 is important to maintain neuronal structural integrity.

Reduced movement alleviates the structural abnormalities of *wts-1*

Neuronal processes contain bundles of microtubules, which are essential structural foundations that protect neurons from mechanical strain-induced damage (Tang-Schomer et al. 2010; Krieg et al. 2017). We hypothesized that the absence of *wts-1* would affect the microtubule stability in some way; thus, physical stresses generated by movement could induce spontaneous degeneration of neurons. To test this hypothesis, we slowed the movement of *wts-1* mutant via the knockdown of muscle machinery genes using RNAi and observed neuronal morphology. As previously reported (MacLeod et al. 1977; Neumann and Hilliard 2014), the knockdown of muscle machinery genes, including a myosin heavy chain gene (*unc-54*), severely impaired organismal movement. Compared with the *wts-1* mutants who were fed with an empty vector (L4440), worms fed with *unc-54* RNAi exhibited uncoordinated movement and some of them were even immobilized (Fig. 4A). Impaired movement resulting from *unc-54* knockdown were also appeared as reduced swimming of animals (Fig. 4E). Consistent with our hypothesis, *unc-54* RNAi resulted in a significant reduction in neuronal swelling/branching events in ALM as well as PLM (Fig. 4B–D). The control ALM showed 7.67 lesions on average, whereas ALM

treated with *unc-54* RNAi had 4.851 lesions at the L4 stage. For PLM, the events of swelling/branching occurred 6.59 times on average in the controls, whereas 2.96 in the *unc-54* RNAi fed neurons at the same stage (Fig. 4C). Additionally, *unc-54* RNAi significantly increased the proportion of intact PLM without any swelling or branching (Fig. 4D). The knockdown of *unc-15* or *unc-95*, which encodes paramyosin (a structural component of thick filaments) and muscle LIM domain protein, respectively (Kagawa et al. 1989; Broday et al. 2004), showed movement defects as well and exhibited ameliorative effects on neuronal structures (Fig. 4E, F). In contrast, *unc-89* and *deb-1* RNAi failed to induce distinguishable movement defects in our experiments (Fig. 4E). As expected, *unc-89* RNAi did not mitigate neuronal swelling in the *wts-1* mutants and *deb-1* RNAi only had limited effects on ALM, and no effect on PLM (Fig. 4F). These observations indicate that the severity of movement defects is inversely correlated with the severity of neuronal deformation and it strongly supports the hypothesis that *wts-1* neurons are vulnerable to physical stresses generated by organismal movements.

Treatment with colchicine, a microtubule-destabilizing agent, reduced ectopic lesions in *wts-1* neurons

For further understanding of the status of microtubules in the *wts-1* mutant neurons, we evaluated the effects of drugs regulating microtubule stability in the mutant neurons. We transferred the *wts-1* mutants to the drug-containing plates at the L4 stage and scored the number of lesions including ectopic swelling and branching along the processes of their L4 stage-offspring. Interestingly, colchicine, a microtubule-destabilizing agent (Vandecandelaere et al. 1997), greatly reduced the morphological abnormalities of the *wts-1* mutant neurons (Fig. 4G). The drug-untreated ALM showed 5.88 swelling/branching events on a process, whereas

the colchicine-treated ALM only had 2.95 swelling/branching. In the case of PLM, colchicine treatment reduced neuronal lesions from 4.41 to 0.89 (Fig. 4H). Structurally intact neurons were significantly increased by colchicine-treatment (Fig. 4I) and the beneficial effect of colchicine on neuronal structures was consistently observed in TRNs of 1DA offspring (Fig. 4J, K). Furthermore, treatment with colchicine significantly improved touch responses of the mutants at L4 stage (Fig. 4L).

In contrast, treatment with paclitaxel, a microtubule-stabilizing agent (Schiff et al. 1979; Vandecandelaere et al. 1997; Yvon et al. 1999), failed to mitigate neuronal abnormalities of the *wts-1* mutants (Supplemental Fig. S4A–C). Because of the poor cuticle permeability of paclitaxel, we introduced a mutation in the *bus-17* gene that encodes galactosyltransferase to damage the cuticle of the *wts-1* mutant, as performed in previous studies (Bounoutas et al. 2009; Neumann and Hilliard 2014). The number of neuronal lesions was comparable between the paclitaxel-treated *wts-1* neurons and untreated controls (Supplemental Fig. S4B). These results show that treatment with colchicine, not paclitaxel, lessened the morphological and functional alteration of *wts-1* neurons, suggesting that hyper-stabilized microtubules are responsible for the structural and subsequent functional decline of the mutant neurons.

Hyper-stabilized microtubules are responsible for age-associated neurodegeneration

Next, we questioned whether colchicine could protect neurons from age-associated morphological alteration in wild-type worms. As colchicine treatment had a detrimental effect on the neurodevelopment of wild-type unlike in case of the *wts-1* mutant (Supplemental Fig. 5A), fully developed worms were transferred to colchicine-containing plates at the first day of adulthood (1DA), and neuronal morphologies were monitored in the same generation to assess

age-associated morphological abnormalities. Among morphological alterations of TRNs, bead-like structures on the PLM did not accrue in the aged worms. Beaded PLM was most frequently observed in the young adults (2DA) and gradually decreased as the worms grew older (Supplemental Fig. 5I). This observation was consistent with the previous study (Toth et al. 2012); thus, we excluded beaded PLM from defective neurons in further analyses.

Notably, both ALM and PLM of colchicine-treated worms maintained intact structures even after 20 days of adulthood (20DA) (Fig. 5A–D). While untreated 20DA had approximately 73.1% and 57.5% defective ALM and PLM, respectively, colchicine-treated worms showed only 23.6% and 7.2% defective ALM and PLM, respectively (Fig. 5C, D). Colchicine treatment significantly reduced multiple structural abnormalities of TRNs, including somatic outgrowth of ALM and ectopic swelling or branching of PLM (Supplemental Fig. 5B–E). However, it failed to mitigate other morphological abnormalities such as beaded process of ALM and somatic outgrowth of PLM (Supplemental Fig. 5F–J). More importantly, colchicine treatment also improved touch responses of aged animals. Whereas there was no difference between touch responses of colchicine-treated and untreated 2DA animals, drug-treated 10DA animals showed significantly higher touch responses compared to the untreated controls (Fig. 5E). However, touch responses of drug-treated 10DA were still lower than those of drug-treated 2DA (Fig. 5E). It seems plausible, given that TRNs of colchicine-treated 10DA were more structurally defective than that of colchicine-treated 2DA (Fig. 5C, D). Considering that the same method of colchicine treatment did not affect worm lifespan (Fig. 5F), the protective effects of colchicine on the structural and functional integrity of TRNs are unlikely to be derived from the prolonged lifespan of worms.

Next, we examined that hyper-stabilization of neuronal microtubules by paclitaxel treatment could mimic aged phenotype of TRNs. Age-synchronized *bus-17(br2)* mutants, in which drug-

permeability was enhanced as mentioned, were transferred to paclitaxel-containing plates at L4 stage and their neuronal morphologies were scored at 5DA stage of the same generation. Although Treatment with paclitaxel did not affect PLM structure, it significantly increased neuronal defects of ALM (Supplemental Fig. 5K, L). Paclitaxel induced beaded processes, somatic outgrowth and cell body abnormalities of ALM, as well as bipolar growth which is reported to be induced by paclitaxel. Taken together, hyper-stabilized microtubules could be responsible for age-related neuronal degeneration and neuronal status of the *wts-1* mutant was similar to that of aged neurons.

Loss of *spas-1*, a putative microtubule-severing enzyme, accelerates structural decline of touch receptor neurons

Spastin, an ATP-dependent microtubule-severing enzyme, is known to cause a human neurodegenerative disease, hereditary spastic paraplegia (HSP) (Hazan et al. 1999; Svenson et al. 2001). Hyper-stabilized microtubules by the loss of spastin activity have been considered as a main contributor of disease pathology (Sherwood et al. 2004; Evans et al. 2005). SPAS-1, the worm homolog of spastin, possesses a microtubule-severing activity and is expressed in the TRNs (Matsushita-Ishiodori et al. 2007; Brown and El Bejjani 2017). We investigated whether hyper-stabilization of microtubules via genetic perturbation of *spas-1* could cause premature structural defects of TRNs as observed in *wts-1* mutant. We found that the *spas-1* mutants exhibit premature deformation of TRNs. From the 2nd day of adulthood (2DA), the mutant ALM displayed an accelerated onset of neuronal deformity (Fig. 6A, C). Although the frequency of defective PLM was not significantly increased in the mutants except in *spas-1(tm683)* at 6DA (Fig. 6D), both the deletion mutants *tm683* and *ok1608* exhibited more various and severe structural deformation of PLM than controls on the 2DA and 6DA (Fig. 6B,

Supplemental Fig. 6A). Ours and others' observation showing touch neuronal expression of SPAS-1 suggest cell-autonomous function of SPAS-1 (Supplemental Fig. 6B) (Brown and El Bejjani 2017). Consistent to the hypothesis, expression of SPAS-1 under *mec-4* promoter, as well as *spas-1* own promoter, restored premature deformation of the *spas-1* mutant ALM (Fig. 6E, F). Human SPAST expression under the control of the *C. elegans spas-1* promoter displayed similar rescue effects, whereas the loss-of-function mutant (K388R), which is associated with disease pathology (Fonknechten et al. 2000), failed to restore the structural integrity of the mutant ALM (Fig. 6E). In the case of PLM, human spastin expression or P*mec-4*-drived Ce_SPAS-1 expression slightly, but not significantly, reduced the structural deformation of the mutants ($p = 0.0502$, $p = 0.1161$, respectively), and other rescue constructs did not affect the PLM structures (Fig. 6E, F).

Next, we investigated that pharmacological destabilization of neuronal microtubules by colchicine treatment could ameliorate structural defects of *spas-1* mutant. As done in *wts-1* mutant background, F1 progenies of animals grown on the drug-contained plate were observed at L4 stage. We found that colchicine treatment not only rescued structural defects of *spas-1* mutant, but also increased touch responses of the mutant at 2DA (Fig. 6G, H).

In human spastin, K388R mutation completely abrogates the ATP binding in the ATPase region and microtubule-severing activity (Evans et al. 2005). Taken together, microtubule-severing activity of SPAST is likely conserved in *C. elegans* SPAS-1 and it is important to protect neuronal structures from gradual deformation. Moreover, the fact that the loss of microtubule-severing enzyme led to accelerated neuronal deformation also supports that hyper-stabilized microtubules are responsible for the age-associated structural decline of neurons.

Loss of microtubule-stabilizing genes *dlk-1* and *ptl-1* delayed premature deformation of *wts-1* neurons

We next studied the genetic interaction between *wts-1* and several genes that are known to regulate microtubule stability, particularly those expected to act in TRNs. We selected six potential microtubule-stabilizing genes (*atat-2*, *dlk-1*, *mec-17*, *mig-2*, *ptl-1* and *ptrn-1*) and five microtubule-destabilizing genes (*kin-18*, *rho-1*, *unc-33*, *spas-1* and *elp-1*). A *wts-1; eri-1* mutant were generated by genetic mating to enhance the efficiency of neuronal RNAi (Kennedy et al. 2004) and we evaluated lesions in the TRNs of worms fed with the RNAi vector of target genes. RNAi against microtubule-stabilizing genes, except for *atat-2* and *mec-17*, could reduce the structural deformation of *wts-1; eri-1* mutant neurons (Supplemental Fig. 7B). *atat-2* RNAi slightly alleviated ectopic lesions in ALM and PLM. *mec-17* RNAi failed to reduce PLM lesions but increased ALM lesions. In contrast, none of the microtubule-destabilizing genes reduced ectopic lesions of the mutant neurons. Among the candidate genes, *rho-1* RNAi resulted in early larval arrest, making it infeasible to test; thus, RNAi experiments were performed for only four genes, which failed to reduce the structural deformation of *wts-1* mutant neurons (Supplemental Fig. 7A).

To address the genetic interaction of microtubule-stabilizing genes and *wts-1* in detail, we constructed double mutants with *wts-1* and *dlk-1*, *ptl-1*, and *ptrn-1*. Both *wts-1; dlk-1* and *wts-1; ptl-1* displayed improved TRNs structures. The total number of ectopic lesions was significantly reduced and the proportion of intact neurons without any deformed structures was also highly increased (Fig. 7A–C). In the case of *ptrn-1*, neuroprotective effects of the gene knockdown were not reproduced in the double mutant (Supplemental Fig. 7C, D). The fact that the loss of microtubule-stabilizing genes mitigates the structural deformation of the *wts-1* also supports the finding that the *wts-1* mutants have highly stabilized microtubules which are

responsible for the structural deformation.

ptl-1 encodes the sole *C. elegans* homolog of the microtubule-associated protein tau (MAPT) (McDermott et al. 1996). In mammals, tau is predominantly localized to the neuronal axons and promotes microtubule assembly and stability; moreover, mutations in the MAPT locus are highly associated with several neurodegenerative diseases, such as FTD-17 (Goedert and Spillantini 2000). In *C. elegans*, the loss of *ptl-1* itself results in premature structural disintegration of TRNs (Chew et al. 2013). Given these observations with the *wts-1; ptl-1* mutants and the revealed functions of MAPT, the structural decline seen in the *ptl-1* mutants is probably due to the microtubule destabilization, unlike those observed in the *wts-1* mutants. Consistent with this assumption, the loss of *yap-1* did not lessen structural deformation of *ptl-1*, even increased the structural abnormalities of *ptl-1* (Fig. 7D, E). On the 5th day of adulthood, *ptl-1* mutant exhibited 41% defective ALM and 6% of defective PLM. In the *ptl-1; yap-1* mutant, cells with irregular shape, ectopic branching or somatic outgrowth were highly increased; thus, 76% ALM and 25% PLM showed structural abnormalities (Fig. 7D, E). Loss of *yap-1* could probably lead to microtubule destabilization and it has a redundant effect on microtubule stability with microtubule destabilization due to *ptl-1* loss.

Discussion

In this study, we showed that the loss of *wts-1*, the core kinase of the Hpo pathway, results in postnatal deformation of TRNs. Although *wts-1* mutants had intact neurons at the beginning, they gradually exhibited structurally and functionally declined TRNs. The detailed observation of morphological alteration in *wts-1* mutant suggests that the features of defective TRNs in the *wts-1* mutant closely resemble those of aged TRNs (Toth et al. 2012). We also defined that

both *yap-1* and *egl-44* act as downstream of *wts-1* and that TRNs-specific rescue of YAP-1 was sufficient to re-induce the neuronal deformation of *wts-1; yap-1* double mutant. Neuronal defects induced by knockdown of *wts-1* or overexpression of YAP-1 selectively in TRNs of wild-type animals also proved a cell-autonomous function of the Hpo pathway in TRNs. Given that *daf-2*/IGF signaling modulates whole organismal aging, premature decline of the *wts-1* mutants is more local and restricted in TRNs. These observations say that the Hpo pathway of *C. elegans* has a neuroprotective effect in differentiated neurons in a cell-autonomous manner, restricting YAP-1 from triggering premature neuronal decline.

In addition to its extensively studied roles in early development and tumorigenesis, dysregulation of the Hpo pathway has been implicated in aging and pathologies of the nervous system (Sahu and Mondal 2020; Gogia et al. 2021). Hyper-activation of the pathway components such as MST1 and the consequent inhibition of YAP have been noted in several neurodegenerative disease models (Matsumoto et al. 2014; Yamanishi et al. 2017; Mueller et al. 2018; Tanaka et al. 2020). In these models, the inactivation of the pathway or the activation of YAP ameliorates neuronal cell death; thus, the manipulation of the Hpo pathway has been regarded to prevent pathologies associated with neuronal cell death. Our results showing that the proper inhibition of YAP-1 by an upstream WTS-1 is required to maintain neuronal integrity appear to contradict these previous observations. However, alterations that occur in the aged brain or the *wts-1* mutants are structural alterations or failures in structural maintenance, which are different from neuronal cell death that occurs in neurodegenerative diseases. This could explain the conflicting function of YAP-1 in terms of neuroprotection. Moreover, some examples present the detrimental effects of uncontrolled YAP. Dysregulation of the pathway and ectopic activation of YAP have been observed in patients with Alexander disease, which is a rare neurodegenerative disease that results in progressive neuronal

degeneration based on the loss of myelin (Wang et al. 2018). Further, the activation of YAP also occurred in Müller cells during retinal degeneration (Hamon et al. 2017). The present study shows that proper regulation of YAP is essential to maintain neuronal integrity and adds important information to the research on anti-aging roles of the Hpo pathway after development.

Genetic and pharmacological approaches suggest that defective, hyper-stabilized microtubules in the *wts-1* mutant were responsible for premature deformation of neurons, possibly in a 'wear-to-tear fashion' because of the mechanical strains generated by organismal movements. Reduced movement or treatment with colchicine had significant ameliorating effects on neuronal deformation of the *wts-1* mutant. Colchicine binds irreversibly to tubulin dimers and prevents the addition of tubulin dimers to the fast growing ends of microtubule (Ravelli et al. 2004). It has been widely used to cure acute gouty arthritis and familial Mediterranean fever (FMF) (Dinarello et al. 1974; Zemer et al. 1974; Zemer et al. 1986). Our study demonstrated that colchicine reduced the severity of neuronal lesions and even improved neuronal function in the *wts-1* mutant TRNs. Moreover, colchicine treatment on fully developed animals largely reduced age-related failures in neuronal structures and functions during normal aging. This supports the idea that neuronal deformation seen in the *wts-1* mutants is similar to that in aged organism and more importantly, hyper-stabilization of neuronal microtubules would be a promising target to cure age-associated neuronal deformation.

These observations are unexpected because microtubule-destabilizing agents mimic several neuronal degenerative disease phenotypes, and microtubule stabilizing agents such as paclitaxel and epothilone D exhibit neuroprotective effects in the pathological contexts (Zhang et al. 2005; Shemesh and Spira 2011; Zhang et al. 2012). Some reports have shown that colchicine has detrimental effects on cognitive function in animal disease models specifically leading to cholinergic neuronal loss (Goldschmidt and Steward 1982; Veerendra Kumar and

Gupta 2002). In contrast, a study in older patients with FMF showed that long-term colchicine treatment could protect against cognitive decline in patients (Leibovitz et al. 2006) and the neuroprotective functions of colchicine also have been reported (Pratt et al. 1994; Salama et al. 2012). In the case of hereditary spastic paraplegia (HSP) and paclitaxel-induced peripheral neuropathy, hyper-stabilization of microtubule could be a cause of neurodegenerative diseases (Cavaletti et al. 1995; Hazan et al. 1999; Trotta et al. 2004; Evans et al. 2005; Lee and Swain 2006; Scripture et al. 2006; Gornstein and Schwarz 2014). Mutated spastin is the most common cause of HSP, a hereditary, neurodegenerative disease that affects the upper motor neurons (Hazan et al. 1999). Similar to the neuroprotective effects of colchicine in the *wts-1* or aged neurons, vinblastine, a microtubule-destabilizing agent, rescue axonal swellings in the HSP models (Fassier et al. 2013). Further, the fact that impaired spastin activity in several animal models results in sparser microtubule array at axons (Sherwood et al. 2004; Wood et al. 2006) provides a possible link between hyper-stabilization and the sparseness of microtubules we observed. These shared properties among *wts-1* mutant neurons, aged neurons and HSP models strongly support that the hyper-stabilized microtubules are responsible for the structural and functional failures of neurons in both senescent and pathological conditions. It will be needed to determine that colchicine has more general neuroprotective effects on age- or diseases-associated decline in other animal models and other microtubule destabilizing agents show similar beneficial effects.

Mutations in several tubulin proteins, microtubule-binding proteins such as tau, and failures in nerve attachment to the epidermis have been reported to induce similar deformities in TRNs, as seen in the *wts-1* mutant. In several mutants of *mec-1*, which encodes an ECM protein, TRNs fail to separate from body-wall muscles and they are prematurely degenerated (Pan et al. 2011). In contrast to the *mec-1* mutant neurons, TRNs of the *wts-1* mutant appeared to normally

dissociate from the muscles and innervate the epidermal layer (Supplemental Fig. S2A). Uncontrolled *yap-1* may affect the vesicular transport of membrane proteins by altering plasma membrane polarity in the same way it acts in the intestine. The detailed mechanism of how the activated YAP-1 triggers microtubule hyper-stabilization in TRNs cell-autonomously remains to be explored. Despite these limitations, the timing of the phenotype of the *wts-1* mutant is noted to be much earlier, and the phenotypic penetrance is much higher in the mutant than in any known mutant. Moreover, to the best of our knowledge, this is the one of the first reports to show the impact of the signaling pathway on the specific neuronal aging. As we have shown in this study, defective TRNs of the *wts-1* mutant could provide a neuronal model to investigate the potential therapeutic targets for improving neuronal aging that occurs either prematurely or normally.

Materials and Methods

Worm maintenance and strains worms were maintained at 20°C as previously described (Brenner 1974), unless noted otherwise. To visualized touch receptor neurons, we isolated *muIs35 [Pmec-7::GFP + lin-15(+)] V* from CF1192 *egl-27(n170) II ; muIs35 [Pmec-7::GFP + lin-15(+)] V* by outcrossing 4 times with N2 wild-type. This strain was used as a wild-type control and *muIs35* was transferred to each mutant background to track touch neurons in all experiment, except that *spas-1* experiments. Since *spas-1* gene is localized at the same chromosome with *muIs35*, CF702 *muIs32[Pmec-7::GFP + lin-15(+)] II* were used as control and transferred in the each mutant background. Exact deletion site of *wts-1(ok753)* was confirmed by PCR. It starts +4025 from ATG start codon and ends +4610. It also has a 'C' insertion after deletion (581bp deletion and 1 insertion). Following strains were used. *wts-1(ok753) I; Ex [Popt-2:: WTS-1::GFP], wts-1(ok753) I; muIs35 V; Ex [Popt-2:: WTS-1::GFP],*

wts-1(ok753) I; muIs35 V; yap-1(tm1416) X, wts-1(ok753) I; egl-44(ys39) II; muIs35 V, wts-1(ok753) I; egl-44(ys41) II; muIs35 V, KP3948 *eri-1(mg366) IV; lin-15B(n744) X,* FX683 *spas-1(tm683) V,* RB1411 *spas-1(ok1608) V,* KU12 *dlk-1(km12) I,* RB809 *ptl-1(ok621) III, ptrn-1(tm5597) X.* CB7431 *bus-17(br2) X,* KP3948 *eri-1(mg366) IV; lin-15B(n744) X.*

Molecular biology Cloning was performed with standard molecular biology techniques. All expressions vector were based on pPD117.01 unless otherwise noted. Primer sequence information is available upon request. To visualize dopaminergic, GABAergic and cholinergic neurons of worms, *dat-1* promoter, *unc-47* promoter, and *cho-1* promoter respectively, were fused to GFP using a standard fusion PCR method.

Fluorescence microscopy To monitor neuronal morphology, a fluorescence microscopy (Axioplan2, Carl Zeiss, Inc) was used. All Fluorescence images were acquired using the confocal microscope (ZEISS LSM700, Carl Zeiss, Inc.) and ZEN software (Carl Zeiss, Inc.).

RNAi For the *unc-54* RNA*i* construct, 2000 bps from 6th exon region was cloned into the L4440 vector. For *unc-95, deb-1, mig-2, mec-17* and *rho-1,* we used constructs from Marc Vidal libraries. The other genes were from the J. Ahringer libraries. RNAi feeding experiments were done by standard methods. 4-6 L4 worms were transferred to plates with bacteria expressing RNAi constructs, neuronal morphology was scored at L4 stage of F1 generations.

Fluorescence microscopy and phenotype scoring To monitor neuronal morphology, a

fluorescence microscope (Axioplan2, Carl Zeiss, Inc) was used. All Fluorescence images were acquired using the confocal microscope (ZEISS LSM700, Carl Zeiss, Inc.) and ZEN software (Carl Zeiss, Inc.) To score mutant phenotype, 30 neuronal cells of stage-synchronized *wts-1(ok753)* mutants were observed for each stage and the experiments were repeated three times. To gain age-synchronized animals, 50 *wts-1* mutants were transferred to the new plate at the first day of adulthood and were removed leaving laid eggs 2 hours later. Since *wts-1(ok753)* develops slower than wild type control, L1 stage worms 16 hours after egg-laying, L2 worms 40 hrs later, L3 worms 54 hrs later and L4 worms 72 hrs later, and 1DA worms after 96hrs were observed. Morphological abnormalities not found in the L4 stage-wild type worms were considered as defects. To quantify phenotype severity of the mutant, total number of ectopic swellings and branching on a neuronal process was measured.

Gentle touch test Touch sensitivity was tested by stroking the animal with an eyebrow hair attached to a toothpick. To test anterior touch response, we stroked around the pharynx of the worm moving forward. In response of touch, the worm moving backward was scored as 'touch sensitive'. In case of posterior touch response, the worm moving backward was tested and tail of the worm was touched.

Drug treatment Colchicine (Sigma-Aldrich, C9754) was added as dry powder into hot agar at 0.1mM concentration. For *wts-1* mutant, 4~5 L4 worms were transferred to plates containing or not containing colchicine. 4 days later, neuronal morphology was scored in their L4 progenies. To monitor colchicine effects on normal aging, we transferred about 300 synchronized 1day adult animals to each plates containing or not containing the drug and

transferred to new plates every 1~2day to remove F1 progenies. At 2, 4, 6, 8, 10, 15, 20 days on their adulthoods, 20 touch neuronal cells were observed. In case of paclitaxel (Sigma-Aldrich, T7402), DMSO was used as the solvent because paclitaxel is poorly soluble in water. Final concentration of paclitaxel is 1μM. Plates only containing DMSO were used as the control. The experiment was performed in the same way as the colchicine treatment into *wts-1*.

Lifespan measurement Lifespan was measured the standard method with some modification. For each strain or condition, 100 L4 worms were transferred to the plates (25 worms per one plate, 4 plates) and living worms were transferred into new plates for every 1~3 days to remove F1 progenies. Worms did not to respond to touch using a platinum wire were scored to be dead. Animals that ruptured from vulva bursting, bagged, crawled off or burrowed into the plates were excluded from the analysis. Every measurement was repeated three times and yielded similar results. One representative experimental result was shown. Statistical analyses were performed using OASIS2 (https://sbi.postech.ac.kr/oasis2/) (Han et al. 2016) and significance were determined by Log-rank (Mantel-Cox) test.

Electron microscopy *C. elegans* animals were overlaid with 20% bovine serum albumin in M9 buffer, and immediately high-pressure frozen using a Leica EM HPM100 apparatus (Leica, Austria). Animals were transferred to the freeze substitution apparatus (Leica EM AFS) under liquid nitrogen into a solution containing 2% osmium tetroxide and 2% water in acetone. Samples were maintained at -90°C for 100 h, slowly warmed to -20°C (5°C per hour) and maintained for 20 h, and slowly warmed to 0°C (6°C per hour). Three washes with cold acetone

were carried out at 0°C and samples were embedded in Embed-812 (EMS, USA). After polymerization of the resin at 60 ˚C for 36 h, serial sections were cut with a diamond knife on an ULTRACUT UC7 ultramicrotome (Leica, Austria) and mounted on formvar-coated grids. Sections were stained with 4 % uranyl acetate for 10 min and lead citrate for 7 min. They were observed using a Tecnai G2 Spirit Twin transmission electron microscope (FEI Company, USA).

References

Barnes AP, Polleux F. 2009. Establishment of axon-dendrite polarity in developing neurons. *Annu Rev Neurosci* **32**: 347-381.

Bishop NA, Lu T, Yankner BA. 2010. Neural mechanisms of ageing and cognitive decline. *Nature* **464**: 529-535.

Bonini SA, Ferrari-Toninelli G, Montinaro M, Memo M. 2013. Notch signalling in adult neurons: a potential target for microtubule stabilization. *Ther Adv Neurol Disord* **6**: 375-385.

Bounoutas A, O'Hagan R, Chalfie M. 2009. The multipurpose 15-protofilament microtubules in C. elegans have specific roles in mechanosensation. *Curr Biol* **19**: 1362-1367.

Brenner S. 1974. The genetics of Caenorhabditis elegans. *Genetics* **77**: 71-94.

Broday L, Kolotuev I, Didier C, Bhoumik A, Podbilewicz B, Ronai Z. 2004. The LIM domain protein UNC-95 is required for the assembly of muscle attachment structures and is regulated by the RING finger protein RNF-5 in C. elegans. *J Cell Biol* **165**: 857-867.

Brown G, El Bejjani R. 2017. SPAS-1 expression in neurons and vulva during L4 stage. *MicroPubl Biol* **2017**.

Cavaletti G, Tredici G, Braga M, Tazzari S. 1995. Experimental peripheral neuropathy induced in adult rats by repeated intraperitoneal administration of taxol. *Exp Neurol* **133**: 64-72.

Chalfie M, Sulston JE, White JG, Southgate E, Thomson JN, Brenner S. 1985. The neural circuit for touch sensitivity in Caenorhabditis elegans. *J Neurosci* **5**: 956-964.

Chalfie M, Thomson JN. 1979. Organization of neuronal microtubules in the nematode Caenorhabditis elegans. *J Cell Biol* **82**: 278-289.

Chew YL, Fan X, Gotz J, Nicholas HR. 2013. PTL-1 regulates neuronal integrity and lifespan in C. elegans. *J Cell Sci* **126**: 2079-2091.

Culotti JG, Merz DC. 1998. DCC and netrins. *Curr Opin Cell Biol* **10**: 609-613.

Dinarello CA, Wolff SM, Goldfinger SE, Dale DC, Alling DW. 1974. Colchicine therapy for familial mediterranean fever. A double-blind trial. *N Engl J Med* **291**: 934-937.

Dong J, Feldmann G, Huang J, Wu S, Zhang N, Comerford SA, Gayyed MF, Anders RA, Maitra A, Pan D. 2007. Elucidation of a universal size-control mechanism in Drosophila and mammals. *Cell* **130**: 1120-1133.

Dubey J, Ratnakaran N, Koushika SP. 2015. Neurodegeneration and microtubule dynamics: death by a thousand cuts. *Front Cell Neurosci* **9**: 343.
Esposito G, Di Schiavi E, Bergamasco C, Bazzicalupo P. 2007. Efficient and cell specific knock-down of gene function in targeted C. elegans neurons. *Gene* **395**: 170-176.
Evans KJ, Gomes ER, Reisenweber SM, Gundersen GG, Lauring BP. 2005. Linking axonal degeneration to microtubule remodeling by Spastin-mediated microtubule severing. *J Cell Biol* **168**: 599-606.
Fassier C, Tarrade A, Peris L, Courageot S, Mailly P, Dalard C, Delga S, Roblot N, Lefevre J, Job D et al. 2013. Microtubule-targeting drugs rescue axonal swellings in cortical neurons from spastin knockout mice. *Dis Model Mech* **6**: 72-83.
Fjell AM, Walhovd KB. 2010. Structural brain changes in aging: courses, causes and cognitive consequences. *Rev Neurosci* **21**: 187-221.
Fonknechten N, Mavel D, Byrne P, Davoine CS, Cruaud C, Bonsch D, Samson D, Coutinho P, Hutchinson M, McMonagle P et al. 2000. Spectrum of SPG4 mutations in autosomal dominant spastic paraplegia. *Hum Mol Genet* **9**: 637-644.
Goedert M, Spillantini MG. 2000. Tau mutations in frontotemporal dementia FTDP-17 and their relevance for Alzheimer's disease. *Biochim Biophys Acta* **1502**: 110-121.
Gogia N, Chimata AV, Deshpande P, Singh A, Singh A. 2021. Hippo signaling: bridging the gap between cancer and neurodegenerative disorders. *Neural Regen Res* **16**: 643-652.
Goldschmidt RB, Steward O. 1982. Neurotoxic effects of colchicine: differential susceptibility of CNS neuronal populations. *Neuroscience* **7**: 695-714.
Gornstein E, Schwarz TL. 2014. The paradox of paclitaxel neurotoxicity: Mechanisms and unanswered questions. *Neuropharmacology* **76 Pt A**: 175-183.
Guo LW, Chen YT, Luo J, Zheng JP, Shao GL. 2019. YAP1 overexpression is associated with poor prognosis of breast cancer patients and induces breast cancer cell growth by inhibiting PTEN. *Febs Open Bio* **9**: 437-445.
Hamon A, Masson C, Bitard J, Gieser L, Roger JE, Perron M. 2017. Retinal Degeneration Triggers the Activation of YAP/TEAD in Reactive Muller Cells. *Invest Ophthalmol Vis Sci* **58**: 1941-1953.
Han SK, Lee D, Lee H, Kim D, Son HG, Yang JS, Lee SV, Kim S. 2016. OASIS 2: online application for survival analysis 2 with features for the analysis of maximal lifespan and healthspan in aging research. *Oncotarget* **7**: 56147-56152.
Harvey KF, Zhang X, Thomas DM. 2013. The Hippo pathway and human cancer. *Nat Rev Cancer* **13**: 246-257.
Hazan J, Fonknechten N, Mavel D, Paternotte C, Samson D, Artiguenave F, Davoine CS, Cruaud C, Durr A, Wincker P et al. 1999. Spastin, a new AAA protein, is altered in the most frequent form of autosomal dominant spastic paraplegia. *Nat Genet* **23**: 296-303.
Hedgecock EM, Culotti JG, Hall DH. 1990. The unc-5, unc-6, and unc-40 genes guide circumferential migrations of pioneer axons and mesodermal cells on the epidermis in C. elegans. *Neuron* **4**: 61-85.
Hirokawa N, Niwa S, Tanaka Y. 2010. Molecular motors in neurons: transport mechanisms and roles in brain function, development, and disease. *Neuron* **68**: 610-638.
Huang J, Wu S, Barrera J, Matthews K, Pan D. 2005. The Hippo signaling pathway coordinately regulates cell proliferation and apoptosis by inactivating Yorkie, the Drosophila Homolog of YAP. *Cell* **122**: 421-434.
Ikegami R, Zheng H, Ong SH, Culotti J. 2004. Integration of semaphorin-2A/MAB-20, ephrin-4, and UNC-129 TGF-beta signaling pathways regulates sorting of distinct sensory rays in C. elegans. *Dev Cell* **6**: 383-395.

Job D, Valiron O, Oakley B. 2003. Microtubule nucleation. *Curr Opin Cell Biol* **15**: 111-117.
Kagawa H, Gengyo K, McLachlan AD, Brenner S, Karn J. 1989. Paramyosin gene (unc-15) of Caenorhabditis elegans. Molecular cloning, nucleotide sequence and models for thick filament structure. *J Mol Biol* **207**: 311-333.
Kang J, Shin D, Yu JR, Lee J. 2009. Lats kinase is involved in the intestinal apical membrane integrity in the nematode Caenorhabditis elegans. *Development* **136**: 2705-2715.
Kennedy S, Wang D, Ruvkun G. 2004. A conserved siRNA-degrading RNase negatively regulates RNA interference in C. elegans. *Nature* **427**: 645-649.
Krieg M, Stuhmer J, Cueva JG, Fetter R, Spilker K, Cremers D, Shen K, Dunn AR, Goodman MB. 2017. Genetic defects in beta-spectrin and tau sensitize C. elegans axons to movement-induced damage via torque-tension coupling. *Elife* **6**.
Lee H, Kang J, Ahn S, Lee J. 2019. The Hippo Pathway Is Essential for Maintenance of Apicobasal Polarity in the Growing Intestine of Caenorhabditis elegans. *Genetics* **213**: 501-515.
Lee JJ, Swain SM. 2006. Peripheral neuropathy induced by microtubule-stabilizing agents. *J Clin Oncol* **24**: 1633-1642.
Leibovitz A, Lidar M, Baumoehl Y, Livneh A, Segal R. 2006. Colchicine therapy and the cognitive status of elderly patients with familial Mediterranean fever. *Isr Med Assoc J* **8**: 469-472.
Liu JY, Li YH, Lin HX, Liao YJ, Mai SJ, Liu ZW, Zhang ZL, Jiang LJ, Zhang JX, Kung HF et al. 2013. Overexpression of YAP 1 contributes to progressive features and poor prognosis of human urothelial carcinoma of the bladder. *BMC Cancer* **13**: 349.
MacLeod AR, Waterston RH, Fishpool RM, Brenner S. 1977. Identification of the structural gene for a myosin heavy-chain in Caenorhabditis elegans. *J Mol Biol* **114**: 133-140.
Maday S, Twelvetrees AE, Moughamian AJ, Holzbaur EL. 2014. Axonal transport: cargo-specific mechanisms of motility and regulation. *Neuron* **84**: 292-309.
Marin O, Valiente M, Ge X, Tsai LH. 2010. Guiding neuronal cell migrations. *Cold Spring Harb Perspect Biol* **2**: a001834.
Matamoros AJ, Baas PW. 2016. Microtubules in health and degenerative disease of the nervous system. *Brain Res Bull* **126**: 217-225.
Matsumoto H, Murakami Y, Kataoka K, Lin H, Connor KM, Miller JW, Zhou D, Avruch J, Vavvas DG. 2014. Mammalian STE20-like kinase 2, not kinase 1, mediates photoreceptor cell death during retinal detachment. *Cell Death Dis* **5**: e1269.
Matsushita-Ishiodori Y, Yamanaka K, Ogura T. 2007. The C. elegans homologue of the spastic paraplegia protein, spastin, disassembles microtubules. *Biochem Biophys Res Commun* **359**: 157-162.
McDermott JB, Aamodt S, Aamodt E. 1996. ptl-1, a Caenorhabditis elegans gene whose products are homologous to the tau microtubule-associated proteins. *Biochemistry* **35**: 9415-9423.
Mueller KA, Glajch KE, Huizenga MN, Wilson RA, Granucci EJ, Dios AM, Tousley AR, Iuliano M, Weisman E, LaQuaglia MJ et al. 2018. Hippo Signaling Pathway Dysregulation in Human Huntington's Disease Brain and Neuronal Stem Cells. *Sci Rep* **8**: 11355.
Neumann B, Hilliard MA. 2014. Loss of MEC-17 leads to microtubule instability and axonal degeneration. *Cell Rep* **6**: 93-103.
Pan CL, Peng CY, Chen CH, McIntire S. 2011. Genetic analysis of age-dependent defects of the Caenorhabditis elegans touch receptor neurons. *Proc Natl Acad Sci U S A* **108**: 9274-9279.

Pratt J, Roux M, Henneguelle E, Stutzmann JM, Laduron PM. 1994. Neuroprotective effects of colchicine in the gerbil model of cerebral ischaemia. *Neurosci Lett* **169**: 114-118.
Ravelli RB, Gigant B, Curmi PA, Jourdain I, Lachkar S, Sobel A, Knossow M. 2004. Insight into tubulin regulation from a complex with colchicine and a stathmin-like domain. *Nature* **428**: 198-202.
Sahu MR, Mondal AC. 2020. The emerging role of Hippo signaling in neurodegeneration. *J Neurosci Res* **98**: 796-814.
Salama M, Ellaithy A, Helmy B, El-Gamal M, Tantawy D, Mohamed M, Sheashaa H, Sobh M, Arias-Carrion O. 2012. Colchicine protects dopaminergic neurons in a rat model of Parkinson's disease. *CNS Neurol Disord Drug Targets* **11**: 836-843.
Schiff PB, Fant J, Horwitz SB. 1979. Promotion of microtubule assembly in vitro by taxol. *Nature* **277**: 665-667.
Scripture CD, Figg WD, Sparreboom A. 2006. Peripheral neuropathy induced by paclitaxel: recent insights and future perspectives. *Curr Neuropharmacol* **4**: 165-172.
Shemesh OA, Spira ME. 2011. Rescue of neurons from undergoing hallmark tau-induced Alzheimer's disease cell pathologies by the antimitotic drug paclitaxel. *Neurobiol Dis* **43**: 163-175.
Sherwood NT, Sun Q, Xue M, Zhang B, Zinn K. 2004. Drosophila spastin regulates synaptic microtubule networks and is required for normal motor function. *PLoS Biol* **2**: e429.
Svenson IK, Ashley-Koch AE, Gaskell PC, Riney TJ, Cumming WJ, Kingston HM, Hogan EL, Boustany RM, Vance JM, Nance MA et al. 2001. Identification and expression analysis of spastin gene mutations in hereditary spastic paraplegia. *Am J Hum Genet* **68**: 1077-1085.
Tanaka H, Homma H, Fujita K, Kondo K, Yamada S, Jin X, Waragai M, Ohtomo G, Iwata A, Tagawa K et al. 2020. YAP-dependent necrosis occurs in early stages of Alzheimer's disease and regulates mouse model pathology. *Nat Commun* **11**: 507.
Tang-Schomer MD, Patel AR, Baas PW, Smith DH. 2010. Mechanical breaking of microtubules in axons during dynamic stretch injury underlies delayed elasticity, microtubule disassembly, and axon degeneration. *FASEB J* **24**: 1401-1410.
Tank EM, Rodgers KE, Kenyon C. 2011. Spontaneous age-related neurite branching in Caenorhabditis elegans. *J Neurosci* **31**: 9279-9288.
Toth ML, Melentijevic I, Shah L, Bhatia A, Lu K, Talwar A, Naji H, Ibanez-Ventoso C, Ghose P, Jevince A et al. 2012. Neurite sprouting and synapse deterioration in the aging Caenorhabditis elegans nervous system. *J Neurosci* **32**: 8778-8790.
Trotta N, Orso G, Rossetto MG, Daga A, Broadie K. 2004. The hereditary spastic paraplegia gene, spastin, regulates microtubule stability to modulate synaptic structure and function. *Curr Biol* **14**: 1135-1147.
Vandecandelaere A, Martin SR, Engelborghs Y. 1997. Response of microtubules to the addition of colchicine and tubulin-colchicine: evaluation of models for the interaction of drugs with microtubules. *Biochem J* **323 (Pt 1)**: 189-196.
Veerendra Kumar MH, Gupta YK. 2002. Intracerebroventricular administration of colchicine produces cognitive impairment associated with oxidative stress in rats. *Pharmacol Biochem Behav* **73**: 565-571.
Wadsworth WG, Bhatt H, Hedgecock EM. 1996. Neuroglia and pioneer neurons express UNC-6 to provide global and local netrin cues for guiding migrations in C. elegans. *Neuron* **16**: 35-46.
Wang L, Xia J, Li J, Hagemann TL, Jones JR, Fraenkel E, Weitz DA, Zhang SC, Messing A, Feany MB. 2018. Tissue and cellular rigidity and mechanosensitive signaling activation in Alexander disease. *Nat Commun* **9**: 1899.

White JG, Southgate E, Thomson JN, Brenner S. 1986. The structure of the nervous system of the nematode Caenorhabditis elegans. *Philos Trans R Soc Lond B Biol Sci* **314**: 1-340.

Wood JD, Landers JA, Bingley M, McDermott CJ, Thomas-McArthur V, Gleadall LJ, Shaw PJ, Cunliffe VT. 2006. The microtubule-severing protein Spastin is essential for axon outgrowth in the zebrafish embryo. *Hum Mol Genet* **15**: 2763-2771.

Yamanishi E, Hasegawa K, Fujita K, Ichinose S, Yagishita S, Murata M, Tagawa K, Akashi T, Eishi Y, Okazawa H. 2017. A novel form of necrosis, TRIAD, occurs in human Huntington's disease. *Acta Neuropathol Commun* **5**: 19.

Yankner BA, Lu T, Loerch P. 2008. The aging brain. *Annu Rev Pathol* **3**: 41-66.

Yuan Y, Li D, Li H, Wang L, Tian G, Dong Y. 2016. YAP overexpression promotes the epithelial-mesenchymal transition and chemoresistance in pancreatic cancer cells. *Mol Med Rep* **13**: 237-242.

Yvon AM, Wadsworth P, Jordan MA. 1999. Taxol suppresses dynamics of individual microtubules in living human tumor cells. *Mol Biol Cell* **10**: 947-959.

Zemer D, Pras M, Sohar E, Modan M, Cabili S, Gafni J. 1986. Colchicine in the prevention and treatment of the amyloidosis of familial Mediterranean fever. *N Engl J Med* **314**: 1001-1005.

Zemer D, Revach M, Pras M, Modan B, Schor S, Sohar E, Gafni J. 1974. A controlled trial of colchicine in preventing attacks of familial mediterranean fever. *N Engl J Med* **291**: 932-934.

Zhang B, Carroll J, Trojanowski JQ, Yao Y, Iba M, Potuzak JS, Hogan AM, Xie SX, Ballatore C, Smith AB, 3rd et al. 2012. The microtubule-stabilizing agent, epothilone D, reduces axonal dysfunction, neurotoxicity, cognitive deficits, and Alzheimer-like pathology in an interventional study with aged tau transgenic mice. *J Neurosci* **32**: 3601-3611.

Zhang B, Maiti A, Shively S, Lakhani F, McDonald-Jones G, Bruce J, Lee EB, Xie SX, Joyce S, Li C et al. 2005. Microtubule-binding drugs offset tau sequestration by stabilizing microtubules and reversing fast axonal transport deficits in a tauopathy model. *Proc Natl Acad Sci U S A* **102**: 227-231.

Zhao B, Wei X, Li W, Udan RS, Yang Q, Kim J, Xie J, Ikenoue T, Yu J, Li L et al. 2007. Inactivation of YAP oncoprotein by the Hippo pathway is involved in cell contact inhibition and tissue growth control. *Genes Dev* **21**: 2747-2761.

Zhao B, Ye X, Yu J, Li L, Li W, Li S, Yu J, Lin JD, Wang CY, Chinnaiyan AM et al. 2008. TEAD mediates YAP-dependent gene induction and growth control. *Genes Dev* **22**: 1962-1971.

Zheng Y, Pan D. 2019. The Hippo Signaling Pathway in Development and Disease. *Dev Cell* **50**: 264-282.

Acknowledgments

We thank the Caenorhabditis Genetics Center and the National BioResource Project for providing strains, Julie Ahringer for RNAi plasmids. We also thank Andrew Fire for the worm expressing vectors. The plasmids containing human SPAST genes were gifts from Jennifer Lippincott-Schwartz (Addgene plasmid #134461, #134463).

Funding

This work was supported by the Samsung Science and Technology Foundation under project Number SSTF-BA1501-52 and National Research Foundation of Korea grant funded by the Korean government (MEST) [2019R1A6A1A10073437]. H. Lee was supported by a scholarship for basic researches, Seoul National University, Seoul, Korea.

Author contributions

Conceptualization: HL, JK, JL

Methodology: HL, JL

Investigation: HL, JK, SL, DL, CHC

Data curation: HL, JL

Supervision: JL

Writing—original draft: HL

Writing—review & editing: HL, JK, JL

Disclosure statement and competing interests

The authors state they have no competing interests or disclosures.

Data and materials availability

All data are available in the main text or the supplementary materials.

Figures

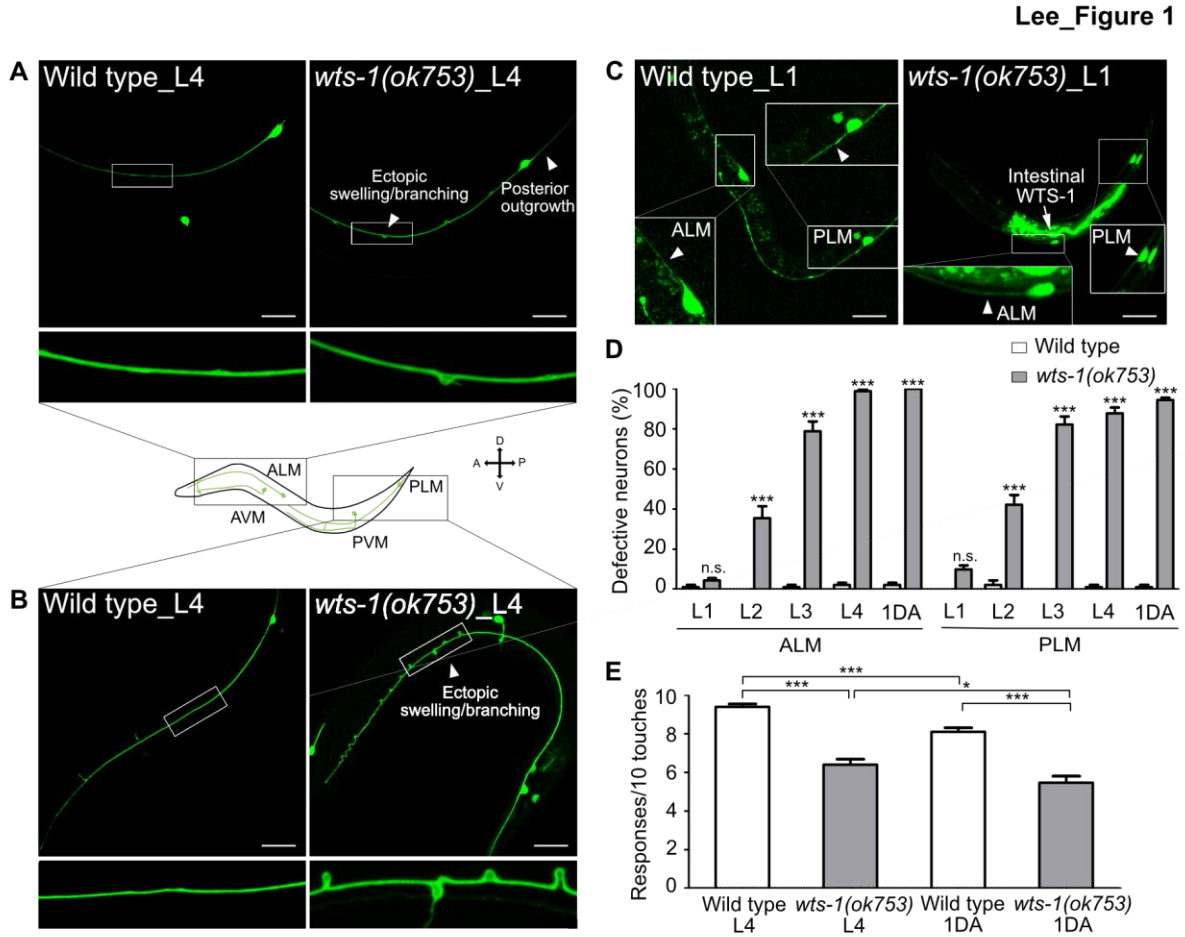

Figure 1. *wts-1* mutants show the premature structural and functional decline of touch receptor neurons (TRNs) (A, B) Representative images of TRNs ([A] ALM and [B] PLM) in the wild-type and *wts-1(ok753)* mutant at the L4 stage. In the mutant, morphologically disrupted ALM and PLM were observed to exhibit abnormalities including ectopic swelling/branching on the processes and posterior outgrowth (arrowheads). (C) Newly developed ALM and PLM in the wild-type and the *wts-1(ok753)* mutant at the early L1 stage. The intact neuronal process is indicated using arrowheads. Intestinal expression of the WTS-1 rescue construct (P*opt-2*::WTS-1::GFP) is indicated using an arrow. (A–C) TRNs were visualized by expressing GFP under the control of the *mec-7* promoter (*muIs35*[P*mec-7*::GFP]) and anterior is to the left unless otherwise noted. Scale bar = 20 µm. (D) Penetration of defective TRNs of the wild-type and the *wts-1(ok753)* at different developmental stages. Neurons displaying any morphological abnormalities such as swelling, branching, somatic outgrowth and extended distal process were scored as defective neurons. In one experiment, 30 cells were observed for each strain and each stage and the experiments were repeated 3 times. Statistical significance was determined by a two-way ANOVA followed by Bonferroni's post-test. (E) Quantified touch responses of the wild-type and the *wts-1(ok753)* mutant at L4 and 1st day of adulthood (1DA). N = 30. Statistical significance was determined by an unpaired t-test. ***, $p < 0.001$, **, $p < 0.01$, *, $p < 0.05$, n.s, not significant, compared to WT or control, unless otherwise marked on graph. All data are presented as means ± SEM, unless otherwise noted.

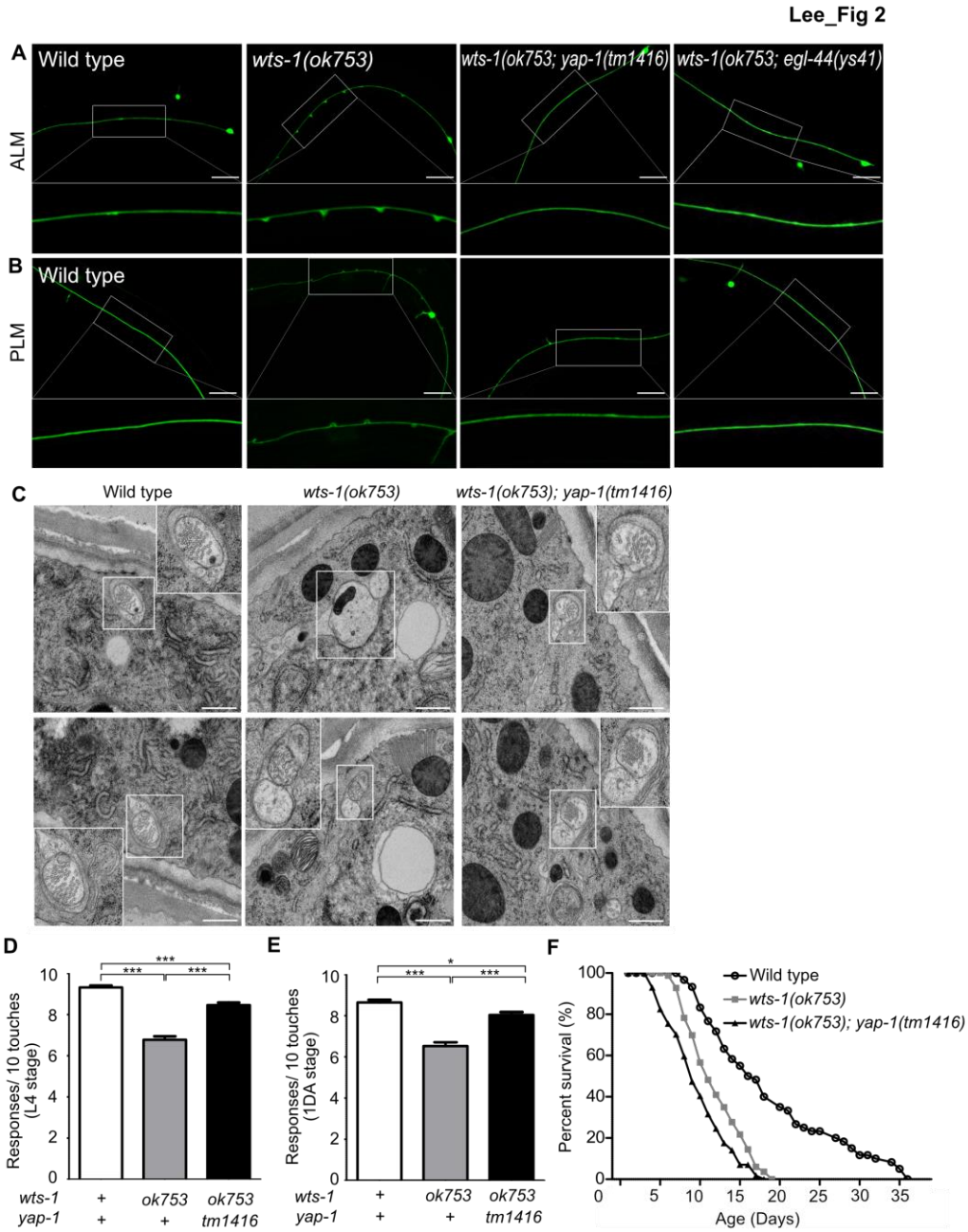

Figure 2. *yap-1* or *egl-44* suppresses premature neuronal decline in *wts-1* mutants. (A, B) Representative images of (A) ALM and (B) PLM in wild-type, *wts-1(ok753)*, *wts-1(ok753); yap-1(tm1416)* and *wts-1(ok753); egl-44(ys41)* at the L4 stage. Loss of *yap-1* or *egl-44* completely restored structural integrity of the *wts-1* mutants. Scale bar = 20 μm. (C) Electron microscope images of wild-type, *wts-1(ok753)* and *wts-1(ok753); yap-1(tm1416)* at 1DA. TRNs are indicated using boxes. Scale bar = 500 nm. (D, E) Touch responses of wild-type, *wts-1(ok753)* and *wts-1(ok753); yap-1(tm1416)* at (D) L4 stage and (G) 1DA stage. For each strain and each stage, 90 animals were tested. Statistical significance was determined using a one-way ANOVA, followed by the Tukey's multiple comparison test. (E) Survival curve of wild-type, *wts-1(ok753)* and *wts-1(ok753); yap-1(tm1416)*. Worms were maintained at 20°C and all lines used for the lifespan analysis have *muIs35*.

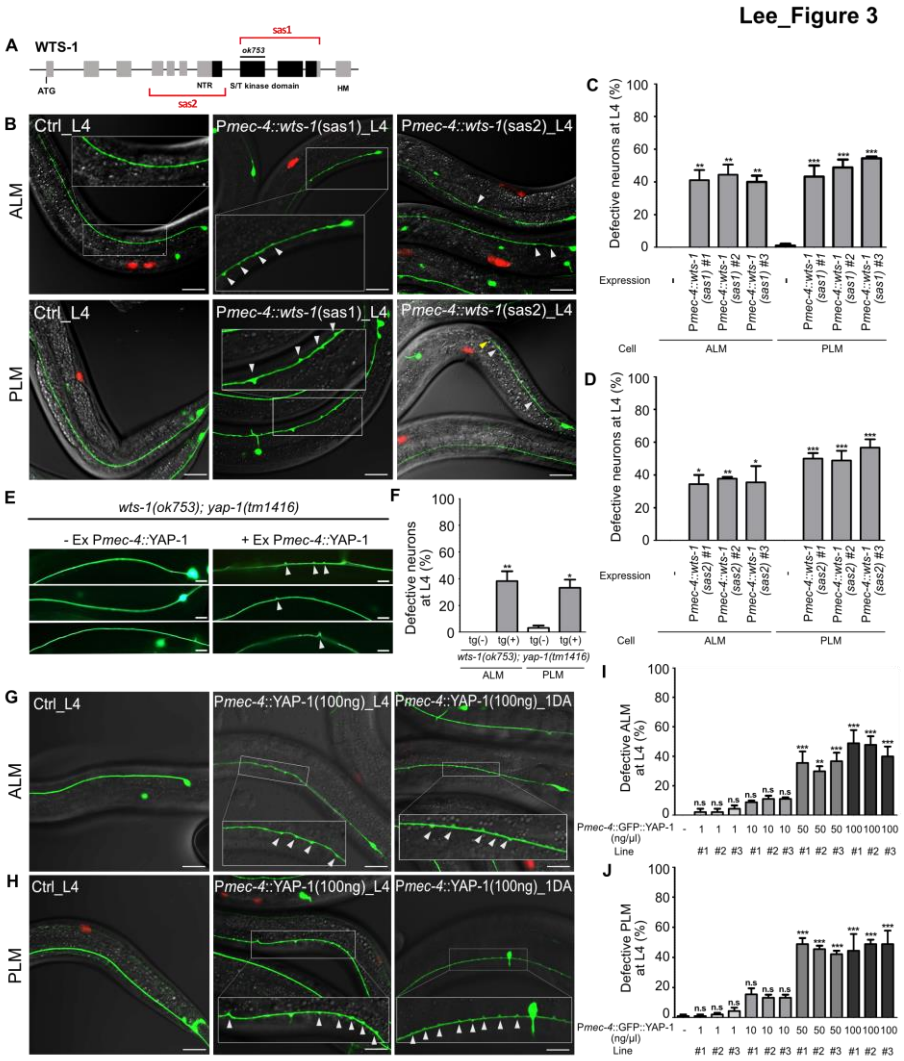

Figure 3. *wts-1-yap-1* act in a cell-autonomous manner to maintain touch neuronal integrity. (A) The targeting regions for touch neuronal specific RNAi of *wts-1*. *S*ense and *a*ntisense (sas) genomic fragments were cloned under the TRNs specific promoter, P*mec-4*. (B) Representative images and (C, D) quantified neuronal abnormalities of TRNs in the controls and *wts-1*-knockdowned animals. Both TRNs-specific-sas1- and sas2-based knock down of *wts-1* efficiently induces neuronal abnormalities as seen in *wts-1* mutant. (E–F) Touch neuronal rescue of YAP-1 is sufficient to re-induce neuronal dis-integrity in *wts-1(ok753); yap-1(tm1416)* mutant. (E) Representative images of TRNs of *wts-1(ok753); yap-1(tm1416)* mutant with the rescue construct or its sibling without transgenes. (F) Quantified results. 60 ALM and PLM of transgenic worms and their siblings were observed. (G, H) Touch neuronal overexpression of YAP-1 is sufficient to induce neuronal abnormalities in wild-type animals. Final concentration of P*mec-4*::GFP::YAP-1 in the injection mixture is 100 ng/μl. (I, J) Quantified neuronal defects of (I) ALM and (J) PLM induced by overexpression of P*mec-4*::GFP::YAP-1 at each concentration in the injection mixtures. (C, D, I, J) 90 ALM and PLM were observed in each of the three independent lines. Neuronal morphology was examined at L4 stage. Statistical significance was determined by a one-way ANOVA followed by the Dunnett's multiple comparison test. An unpaired t-test was used for (F). Red: Expression of injection marker, P*unc-122*::RFP, white arrowhead :neuronal swelling, yellow arrowhead: shortened process. Scale bar = 20 μm.

Lee_Fig 4

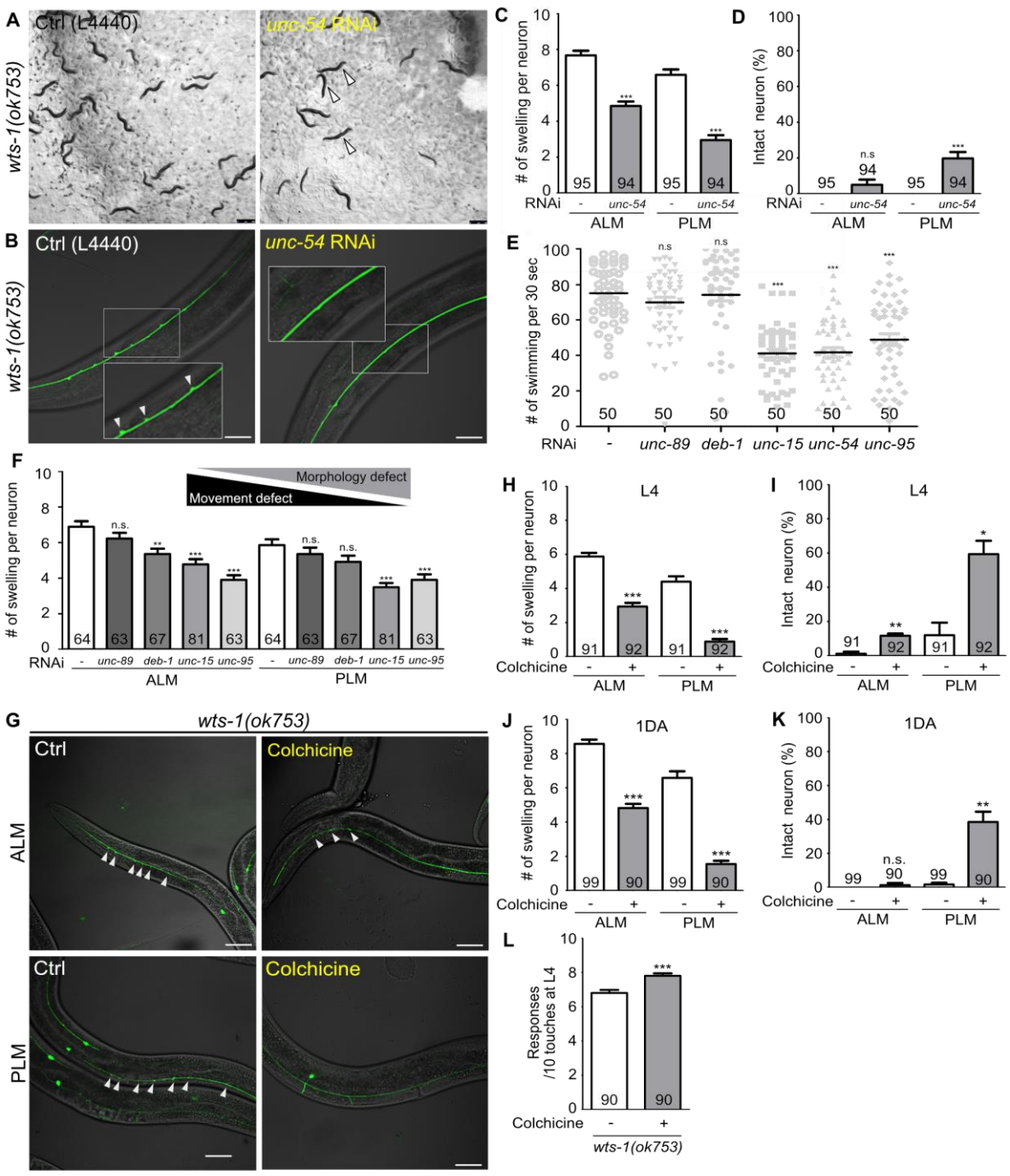
A
Ctrl (L4440)
unc-54 RNAi
wts-1(ok753)
B
Ctrl (L4440)
unc-54 RNAi
wts-1(ok753)
C
# of swelling per neuron
RNAi
ALM
PLM
D
Intact neuron (%)
E
# of swimming per 30 sec
RNAi
unc-89
deb-1
unc-15
unc-54
unc-95
F
Morphology defect
Movement defect
# of swelling per neuron
ALM
PLM
G
wts-1(ok753)
Ctrl
Colchicine
ALM
PLM
H
L4
# of swelling per neuron
Colchicine
I
L4
Intact neuron (%)
J
1DA
# of swelling per neuron
K
1DA
Intact neuron (%)
L
Responses /10 touches at L4
wts-1(ok753)

Figure 4. Abnormal microtubules are responsible for neuronal dis-integrity observed in the *wts-1* mutants. (A–D) Reduced movement resulting from *unc-54* knockdown diminishes ectopic swelling or branching in the *wts-1(ok753)* mutant. (A) *unc-54* knockdown leads to uncoordinated movement of worms (yellow arrowhead). (B–C) *unc-54* knockdown reduces the number of neuronal lesions on the ALM and PLM. (D) *unc-54* knockdown slightly, but significantly, increases the percentages of intact PLM and not ALM. Neurons without any structural defects, including swelling or branching, were considered intact. (E) Quantified motor deficits in animals knocking down various muscle machinery genes. RNAi against *unc-15, unc-54* or *unc-95* impaired swimming behavior, whereas *unc-89* and *deb-1* made no differences compared to control. (F) Quantified morphological abnormalities of TRNs in muscle machinery-knockdown animals. Knockdown of *unc-89* or *deb-1* did not alleviate structural decline of both ALM and PLM. (G–K) Treatment with colchicine reduces ectopic neuronal swelling and increases the percentages of intact neurons in the *wts-1(ok753)* mutants. F1 progenies grown on the drug-contained plates were scored at (H, I) L4 stage or (J, K) 1DA. (L) Colchicine treatment improved touch responses of *wts-1* mutant. The behavior test was done at L4 stage. Statistical significance was determined using an unpaired t-test (C, D, H, L) or a one-way ANOVA, followed by the Dunnett's multiple comparison test (E, F). The total number of cells or animals analyzed is indicated in each column. Asterisks indicate differences from L4440-fed or drug-untreated-control neurons. Ectopic neuronal swelling and branching were labeled with white arrowheads. Scale bar = 20μm.

Lee_Fig 5

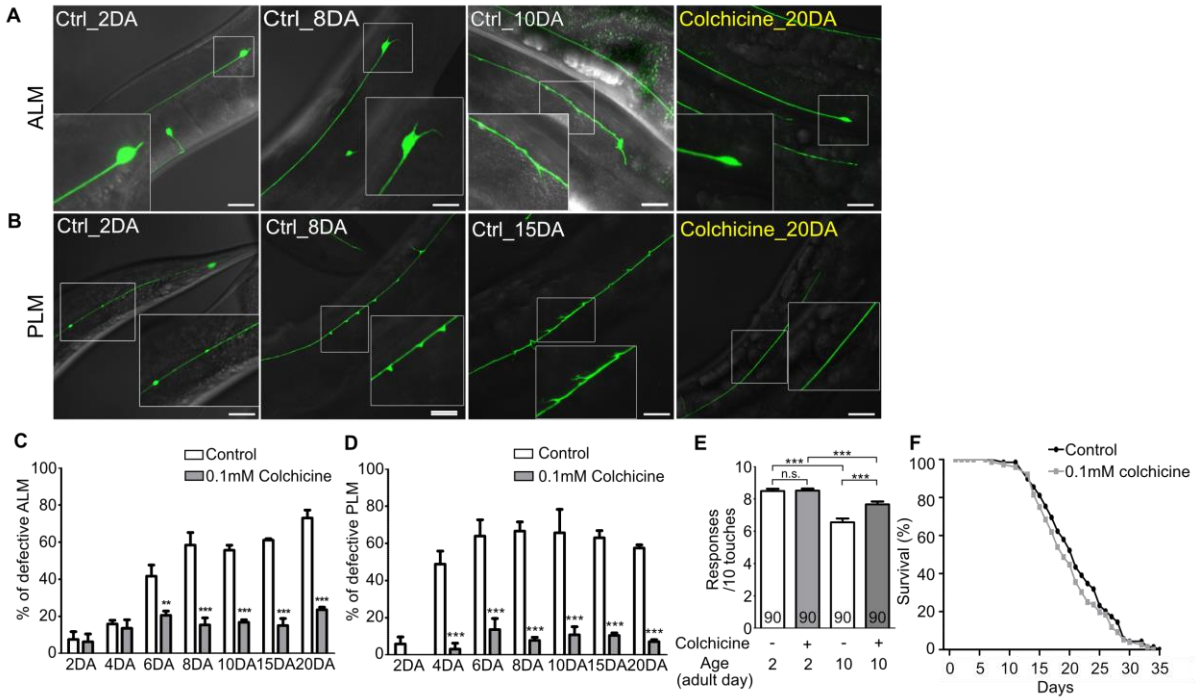

Figure 5. Hyper-stabilized microtubules might be responsible for age-associated morphological deformation of touch receptor neurons. (A, B) Representative images of (A) ALM and (B) PLM of colchicine-treated or untreated wild-type worms. The age of worms is indicated in the image. (C, D) Quantified defects of (C) ALM or (D) PLM in colchicine-treated or untreated worms. Age-synchronized worms were transferred to drug-containing plates on the 1DA and phenotypes were scored on every 2nd, 4th, 6th, 8th, 10th, 15th and 20th day of adulthood. At every time point and in each group, 20 neurons were scored per one experiment and the experiments were repeated 3 times. (E) Colchicine treatment alleviates impaired touch responses of aged animals. Touch responses were scored at 2DA and 10DA. Statistical significance was determined by a two-way ANOVA, followed by the Bonferroni's post-tests (C, D) or a one-way ANOVA with the Bonferroni's multiple comparison test (E). (F) Survival curves of colchicine-treated and untreated control animals. Scale bar = 20μm.

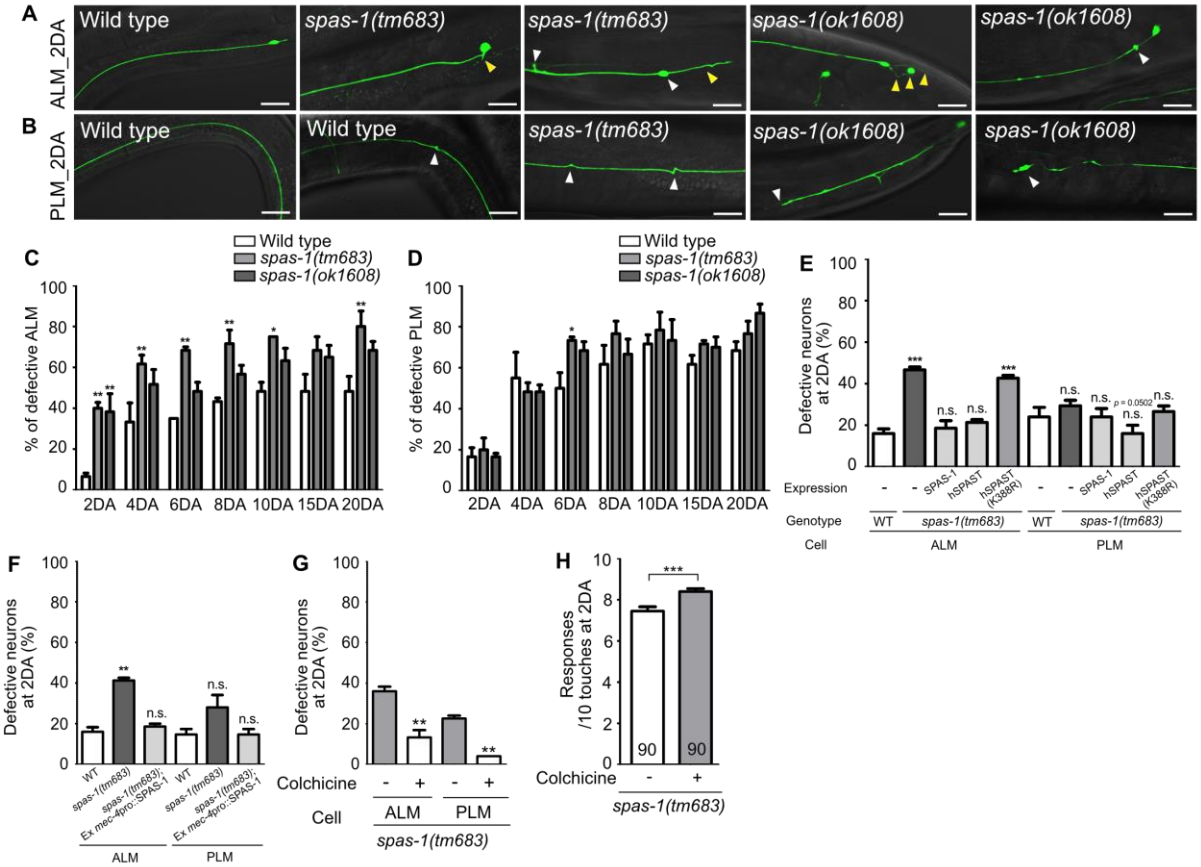

Figure 6. Loss of *spas-1*, a microtubule-severing enzyme, results in premature structural decline. (A, B) Representative images of defective TRNs of *spas-1* mutant on the 2DA. Both deletion mutants, *tm683* and *ok1608*, displayed age-associated morphological alterations of ALM or PLM including ectopic swelling and branching on the neuronal process (white arrowhead), somatic outgrowth and irregular shape of the cell body (yellow arrowhead) precociously. (C, D) Quantified results of structural defects of ALM or PLM in *spas-1* mutants. At every time point, 20 neurons were scored and the experiments were repeated 3 times. (E) Results of the rescue experiment of premature neuronal degeneration of *spas-1(tm683)* with SPAS-1, human SPAST(wt) and human SPAST(K388R). In all cases, the *C. elegans spas-1* promoter was used to induce the C-terminally mCherry tagged transgene. (F) Touch neuronal specific expression of SPAS-1 was sufficient to rescue neuronal defects of ALM. (E–F) Neuronal morphology were scored at 2DA. For each rescue construct, three independent transgenic lines were observed that yielded similar results and the results of one line are presented. (G, H) Quantified (G) structural defects of TRNs or (H) touch responses of colchicine-treated and untreated *spas-1(tm683)* mutant. Analyses were done at 2DA (N =30/one experiment, repeated 3times). Statistical significance was determined using a two-way ANOVA, followed by the Bonferroni's multiple comparison test (C–D), a one-way ANOVA with the Dunnett's multiple comparison test (E–F) or with the Turkey's multiple comparison test (G). Unpaired t-test was used in (H). Scale bar = 20 μm.

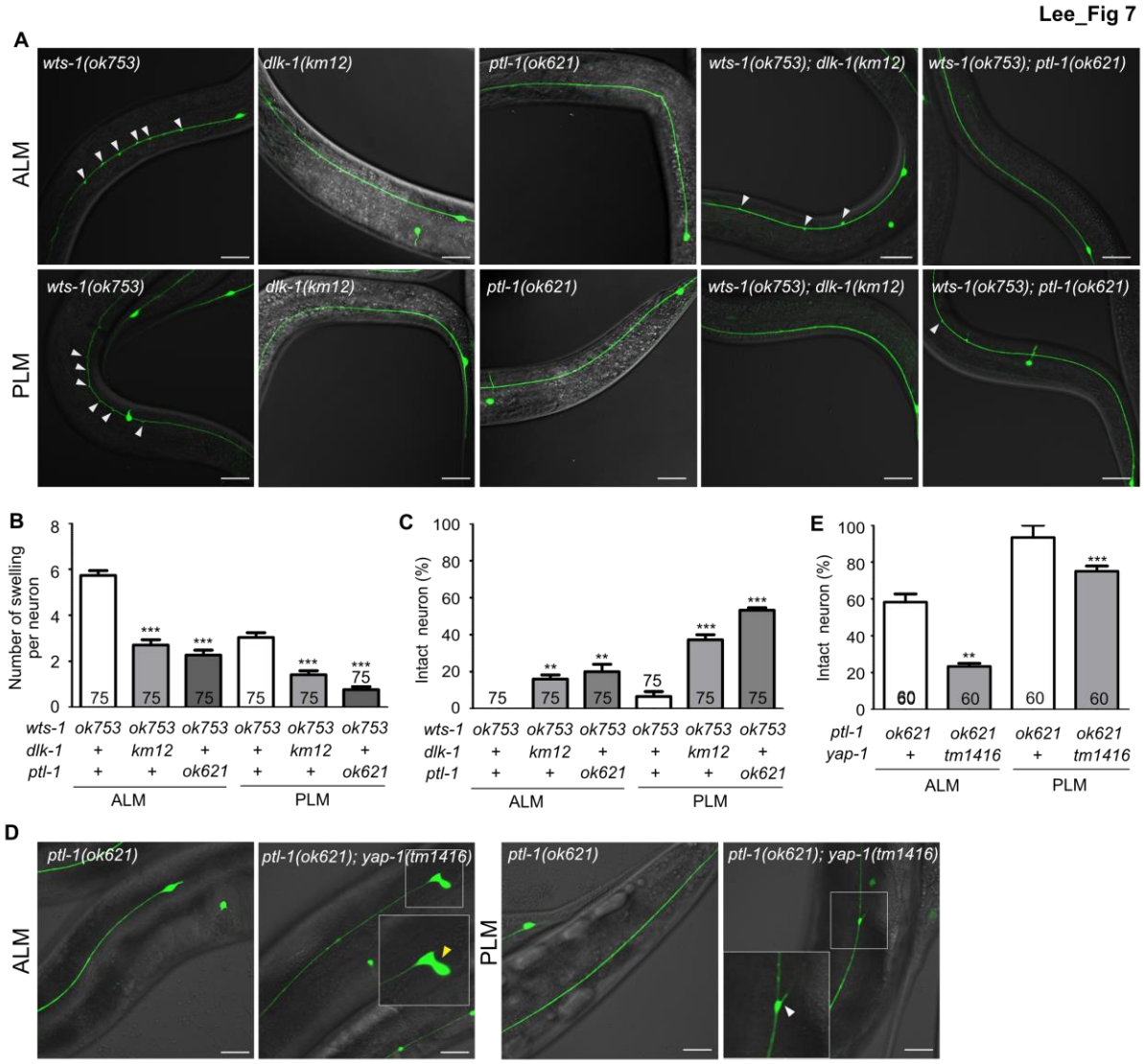

Figure 7. *wts-1-yap-1* affect neuronal integrity possibly by modulating microtubule stability (A–C) Loss of *dlk-1* or *ptl-1* significantly mitigates the structural deformation of *wts-1*-mutant neurons. (A) Representative images of ALM (upper panels) and PLM (lower panels) of *wts-1(ok753), dlk-1(km12), ptl-1(ok621), wts-1(ok753); dlk-1(km12)* and *wts-1(ok753); ptl-1(ok621)* at L4 stage. Ectopic lesions were labeled with arrowhead. (B) Average number of ectopic lesions per neuronal process of each strain. (C) Percentage of intact neurons of each mutant. Loss of *dlk-1* or *ptl-1* protects TRNs of the *wts-1* from premature deformation. (D, E) Loss of *yap-1* worsen the neuronal deformation as seen in the *ptl-1* mutant. (D) Unlike *ptl-1(ok621)* single mutant, *ptl-1(ok621); yap-1(tm1416)* double mutant exhibits severe deformation in ALM and PLM, such as irregular shape of cell body (yellow arrowhead) and ectopic branching (white arrowhead) of the neuronal process. (E) Percentage of undamaged touch neurons in *ptl-1(ok621)* and *ptl-1(ok621); yap-1(tm1416).* (A–E) Neurons were analyzed at the L4 stage. The number of scored neurons is indicated in each column. Statistical significance was determined using a one-way ANOVA, followed by the Dunnett's multiple comparison test. Asterisks indicate differences from the *wts-1* or the *ptl-1* single mutant. Scale bar = 20 μm.

Supplemental Figure legends

Figure S1. Loss of *wts-1* leads to touch neuronal-specific structural decline. (A, B) Various morphological deformations observed in *wts-1* mutant (A) ALM, (B) PLM. In the mutants, both ALM and PLM showed ectopic swelling (a), branching (b) and somatic outgrowth (c). ALM also displays an extended distal process (d), posterior outgrowth (e), or abnormalities in the cell body (f). PLM exhibits extended (g) or shortened (h) process. TRNs were analyzed at the L4 or 1st day of adulthood (1DA) stage. Intestinal expression of the WTS-1 rescue construct is indicated using a yellow arrowhead. (C) Structural decline of AVM and PVM in the *wts-1* mutants. Somatic outgrowth or ectopic branching/swelling on the process is occasionally noted in both AVM and PVM. (D) Quantified structural defects of AVM and PVM in wild-type and *wts-1* mutants at different stages. Statistical significance was determined using a two-way ANOVA followed by Bonferroni's post-test. (E–H) Quantified structural defects of ALM and PLM observed in *wts-1* mutants at different stages. (D) Ectopic swelling or (E) branching on the neuronal process occurs the most frequently, followed by (F) somatic outgrowth and (G) extended distal process. Structural deformations of each category tend to increase as the worms grow. (I) The average number of ectopic lesions on a neuronal process of ALM or PLM of *wts-1* at different stages. The total number of ectopic swelling or branching was scored. (D–I) At each time point, 90 ALM or PLM were analyzed (N=30, repeated 3 times). (J) Representative images of dopaminergic, GABAergic and cholinergic neurons in *wts-1* mutants at the L4 stage. Each neuron was visualized using a fluorescent marker under the control of a specific promoter; *dat-1* promoter, *unc-47* promoter, *cho-1* promoter, respectively. (K) Quantified structural defects of dopaminergic, GABAergic and cholinergic neurons in wild-type and *wts-1* mutants. N = 90. ***, $p < 0.001$, **, $p < 0.01$, *, $p < 0.05$, n.s, not significant, compared to WT or control, unless otherwise marked on graph. All data are presented as means ± SEM, unless otherwise noted. Scale bar = 20μm.

Figure S2. *yap-1* suppresses structural deformities of *wts-1* mutant neurons. (A) Electron microscope images shows that TRNs (ALM) normally dissociate from the muscles (M) and innervate the epidermis in the *wts-1* mutants. TRNs are indicated using boxes. Scale bar = 1 μm. (B–D) Microtubules of TRNs in (B) control wild-type, (C) *wts-1(ok753)* and (D) *wts-1(ok753); yap-1(tm1416)*. Decreased number of microtubules in *wts-1* mutant ALM was restored in *wts-1(ok753); yap-1(tm1416)*. Microtubules are indicated using red numbers and the total number of microtubules present in each section is indicated in the upper left area of

each image. Imaging was performed at 1DA. Sections were cut from the head and serial sections for 5~10 μm of one individual are presented. Scale bar = 500 nm.

Figure S3. Cell-autonomous function of *wts-1*. (A) Representative images of ALM (upper panels) and PLM (lower panels) of control animals and *wts-1* TRNs-specific-knockdown animals at 1DA. Both sas1 and sas2 constructs effectively induced structural defects in TRNs. Ectopic neuronal swelling was labeled with white arrowheads and other structural defects, including abnormal cell body, shortened process of PLM were labeled with yellow arrowheads. (B, C) Quantified neuronal defects induced by (B) sas1- or (C) sas2-based knockdown of *wts-1*. Neurons were observed at 1DA. N=30/one experiment, repeated 3 times. Statistical significance was determined by a one-way ANOVA, followed by the Dunnett's multiple comparison test. Scale bar = 20μm.

Figure S4. Paclitaxel treatment fails to mitigate *wts-1* neuronal defects. (A) Representative images of ALM (upper panels) and PLM (lower panels) of *wts-1* mutants treated with paclitaxel and untreated control worms. Unlike colchicine treatment, paclitaxel treatment failed to lessen the touch neuronal deformation of the mutants. (B) Quantified results of ectopic neuronal lesion scoring. In total, 60 cells were analyzed for each neuron. (C) Quantified results of the percentage of intact ALM and PLM in the *wts-1(ok753); bus-17(br12)* under the condition of paclitaxel-treated and untreated worms. Statistical significance was determined using an unpaired t-test. Ectopic neuronal swelling was labeled with arrowheads. Scale bar = 20μm.

Figure S5. Colchicine treatment affects touch receptor neurons morphology. (A) Representative images of TRNs of 8-day-old adult wild-type worms fed with colchicine from parental generations. Arrowheads indicate highly degenerated touch receptor neurons of F1 progenies. Almost all processes of ALM or PLM degraded and the cell bodies showed exhibit irregular shape. (B–J) Quantified results of the effect of colchicine on age-related structural deformations of touch neurons in each category. Colchicine (0.1 mM) was used on worms from the 1DA and phenotypes were scored at every 2nd, 4th, 6th, 8th, 10th, 15th and 20th day of adulthood (N =20/one experiment, repeated 3 times). Among the structural deformations, some features which are particularly associated with age, such as (B) somatic outgrowth and (C) posterior outgrowth of ALM or (D) swelling and (E) branching of PLM have been significantly reduced by colchicine-treatment. Colchicine-treatment has only limited effects on (G) branching of ALM or no effect on (H–J) the other deformations. Statistical differences were determined using a two-way ANOVA, followed by the Bonferroni's post-test. Asterisks

indicate differences from untreated control ALM or PLM. (K, L) Paclitaxel treatment significantly increases neuronal defects of ALM. (K) Representative images of TRNs of control animals and paclitaxel-treated animals at 5DA. (L) Quantified neuronal defects in controls and drug-treated animals (N=30/one experiment, repeated 3times). Statistical significance was determined using an unpaired t-test. Scale bar = 20 μm.

Figure S6. *spas-1* also act cell autonomously to maintain neuronal morphology of TRNs. (A) Both *spas-1* deletion mutants displayed structural decline of TRNs precociously. Neurons were imaged at 6DA. Neuronal abnormalities were labeled with arrowheads. (B) SPAS-1 expressed in TRNs (Red: P*spas-1*:: *spas-1*:: mCherry, Green: P*mec-7*::GFP). Scale bar = 20μm.

Figure S7. Microtubule destabilizing genes, not stabilizing genes, mitigate morphological deformations of *wts-1* mutant neurons. (A, B) Knockdown of genes required for microtubule stabilization, except for *mec-17*, lessen the morphological abnormalities of *wts-1* mutant neurons. In contrast, the knockdown of genes acting as microtubule destabilizers did not affect the *wts-1* neuron. (C) ALM and PLM of the *wts-1(ok753); ptrn-1(tm5597)*. Unlike *dlk-1* or *ptl-1*, the *wts-1; ptrn-1* double mutant failed to recapitulate the knockdown effect of *ptrn-1*. Arrowheads labeled neuronal lesions. (D) Average number of the total ectopic lesions per neuronal process of the *wts-1; ptrn-1* mutant. (A–D) ALM or PLM at the L4 stage was scored. Statistical significances were determined by a one-way ANOVA, followed using the Dunnett's multiple comparison test. Asterisks indicate differences from L4440-fed ALM or PLM (A, B) or the *wts-1* single mutant neurons (D). Scale bar = 20μm.